IEEE Access
Multidisciplinary | Rapid Review | Open Access Journal

Received December 11, 2017, accepted January 21, 2018, date of publication February 21, 2018, date of current version March 16, 2018.

Digital Object Identifier 10.1109/ACCESS.2018.2808414

Impact of Nonlinear RFI and Countermeasure for Radio Astronomy Receivers

MAHMOUD E. ABDELGELIL, (Student Member, IEEE), AND HLAING MINN, (Fellow, IEEE)
Department of Electrical and Computer Engineering, The University of Texas at Dallas, Richardson, TX 75080, USA

Corresponding author: Mahmoud E. Abdelgelil (mahmoud.abdelgelil@utdallas.edu)

This work supported by the National Science Foundation under Grant 1547048.

ABSTRACT Radio frequency interference (RFI) has become a critical issue to radio astronomy system (RAS) due to fast-expanding active wireless systems. A recent solution based on a coexistence paradigm offers some RFI-free durations for RAS but further expansion of RAS observation needs to cope with strong RFI. To enhance spectrum access opportunities for both wireless communications and RAS, we explore a new approach where both the systems simultaneously access the spectrum for some durations and RAS exploits RFI cancellation. The main challenge is the nonlinear distortion caused by strong RFI. We develop a signal model incorporating the nonlinearity effect and study its impact on RAS observation performance. We propose an auxiliary receiver assisted nonlinear-RFI cancellation scheme and a modified RAS signal detection scheme. Furthermore, we develop two channel estimators (unscented Kalman filter-based approach and nonlinear-to-linear mapping approach) for nonlinear systems which we apply in our RFI cancellation scheme. Analytical and numerical performance evaluation results show substantial performance advantage of our proposed methods and illustrate importance of incorporating nonlinearity in the channel estimation, RFI cancellation, and RAS signal detection.

INDEX TERMS RFI, UKF, interference cancellation, non-linearity, radio astronomy, non-linear to linear mapping.

I. INTRODUCTION

Radio spectrum is one of the most valuable natural resources and its usage can be divided into active and passive categories. The active one includes wireless transmission systems such as cellular wireless communications (CWC), Wi-Fi and satellite communications. The passive one corresponds to receive-only systems such as radio astronomy system (RAS). RAS detects astronomical signals from the space and its signal to noise ratio (SNR) can be as low as -60 dB [1]. Thus, RAS is very sensitive to radio frequency interference (RFI) and receiver noise. To cope with the noise sensitivity, very low-noise amplifiers (LNAs) have been developed for RAS [2]–[8]. To avoid RFI, RAS receivers are located in remote areas, typically surrounded by radio quiet zones. However, phenomenal growth of active wireless systems causes less spectrum access opportunities for RAS due to increasing RFI across time, frequency, and space. Due to the importance of RAS to science and society, the international telecommunication union (ITU) allocated some frequency bands to RAS and set some regulations and recommendations to protect RAS [1], [9]–[12]. However, RAS generally needs astronomical observations in almost all available atmospheric windows ranging from 2 MHz to 1000 GHz and above. Thus, the issue of conflicting spectrum needs becomes more critical as both active and passive wireless systems expand.

Since both types of wireless services provide benefits to the society, their growth and coexistence are important. In view of such needs and conflicts, recently [13] and [14] proposed a shared spectrum access paradigm between CWC and RAS. With some coordination between the two systems, a three-phase time division spectrum access is developed within a shared spectrum access zone, where both systems can geographically coexist without requiring radio quiet zones. This scheme uses three time intervals for CWC only phase, CWC+RAS phase, and RAS only phase within each time frame. The CWC+RAS phase has two main purposes - i) for absorbing different propagation times of active wireless transmitters so that no RFI occurs during the RAS only phase and ii) for fine tuning of the shared spectrum access zone/frame structure and synchronization. For better spectrum utilization, the three phases can be designed with different intervals across time according to the time-dependent average

wireless traffic statistics of CWC. However, as spectrum needs of both systems increase, more aggressive strategies beyond the above time division sharing will be needed in the future. Exploiting tremendous advances in signal processing capabilities, a plausible approach for obtaining further spectrum access opportunities for RAS is to develop a system with advanced RFI cancellation under simultaneous spectrum access scenarios. It can be applied during the CWC only phase of the scheme in [13] and [14] or at specific RAS receivers where RFI cancellation is needed due to planned or unplanned RFI.

RFI mitigation plays an important role for RASs [15]–[17]. In [18] a new approach is introduced that uses an auxiliary receiver to detect the interference, and then by using a least mean square (LMS) filter, it removes the interference. In [19] the same technique is used on a different application with a larger filter length. In [20] a post correlation cancellation is introduced instead of a pre-correlation cancellation. All of these existing RFI mitigation methods do not consider nonlinearity at the low noise amplifier (LNA). Even in the current paradigm, sometimes unintentional strong RFI could enter into RAS receiver. For our explored scenario of simultaneous spectrum access between CWC and RAS, RFI would be much stronger, thus driving the RAS's LNA into a non-linear region. This creates a much more challenging RFI mitigation problem due to the non-linearity, and the existing approaches would not be effective. In this paper, we propose an efficient solution to such problem.

Our contributions are summarized below.

1) We develop a new signal model which incorporates non-linearity effects of LNA and analyze how RFI in the LNA non-linear region affects the performance of the RAS signal power detection using an existing detector.
2) We propose a nonlinear-RFI cancellation scheme and a modified RAS signal power detection scheme based on the above analytical development.
3) With the aid of a reference/auxiliary receiver, we develop an unscented Kalman filter (UKF) based approach [21]–[23] to estimate the channel of the interference to RAS under nonlinearity, which is to be used in the RFI cancellation and detection schemes.
4) For the above channel estimation task in the same system setting, we develop another novel channel estimator based on a nonlinear-to-linear mapping (NL-L).
5) We derive closed-form analytical expressions which characterize the performance of the proposed RAS signal detector under nonlinearity.
6) We conduct numerical performance comparisons of the proposed and existing approaches for channel estimation and RAS signal detection under nonlinearity effects and illustrate the performance advantage of the proposed approaches under different channel models and RFI modulations.

We presented an earlier development covering the first three contributions in a conference paper [24].

The paper is organized as follows. Section II describes the RAS system model with linear and nonlinear LNA and shows the effects of nonlinearity. Section III presents our proposed method for compensating the non-linearity effects and interference estimation using UKF and the new NL-L mapping with excision. Section IV includes a detailed analysis for the performance of the proposed RAS signal power detection. Section V covers numerical performance evaluation results and discussions. Section VI draws conclusions.

Throughout the paper the superscripts T and H represent the transpose and conjugate transpose operations. The subscripts bb, r and i refer to the baseband equivalent, real part and imaginary part, respectively. $\Re\{X\}$ and $\Im\{X\}$ denote the real and imaginary parts of X. The time averaging for $x[k]$ over m samples is denoted by $\overline{x[k]} = \frac{1}{m}\sum_m x[k]$ and $\hat{x}$ means the estimate of x. For the convenience of reading, we list abbreviations in Table 1.

TABLE 1. List of abbreviations.

Abbreviation	Definition
CIR	Channel impulse response
CWC	Cellular wireless communications
ITU	International telecommunication union
KF	Kalman filter
LMS	Least mean square
LNA	Low noise amplifier
LS	Least square
NL-L	Nonlinear-to-linear mapping
QAM	Quadrature amplitude modulation
QPSK	Quadrature phase-shift keying
RAS	Radio astronomy system
RFI	Radio frequency interference
UKF	Unscented Kalman filter

II. SYSTEM MODEL

Radio astronomy systems detect the power of an astronomical signal in a desired bandwidth. The main challenge is that the signal is extremely weak, much below noise level, and is highly sensitive to RFI that comes from different radio sources. RFI negligible to CWC could be strong enough to disrupt RAS observations. Unintended RFI due to an imperfect system design or faulty devices could yield strong RFI to RAS. Similarly, in a simultaneous spectrum access scenario between CWC and RAS, RFI to RAS will be strong. Thus, we consider scenarios with strong RFI. We use an auxiliary (reference) receiver assisted RAS receiver similar to [18], but the difference is the incorporation of nonlinearity effects in our work. Fig. 1 shows the composition of such an RAS receiver, where the auxiliary receiver assists the main receiver in the RFI cancellation process. The reference receiver antenna is steered toward the direction of interference in order to improve the detection performance of the interference signal, which is used in the main RAS receiver's RFI cancellation process. In this section, we describe the signal detection (power estimation) mechanism of the RAS and evaluate its performance when the LNA operates in linear and nonlinear regions.

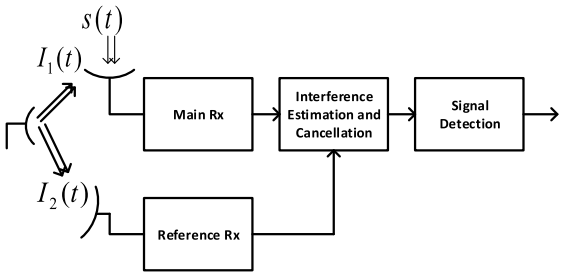

FIGURE 1. RAS receiver with auxiliary receiver assisted RFI cancellation.

A. RAS SIGNAL DETECTION IN A LINEAR SYSTEM

In this subsection, we present the RAS signal detection when the system behaves linearly. From Fig. 1, the received signal at the main receiver contains an RAS signal $s(t)$ and an RFI signal $I_1(t)$. The RAS receiver adds a noise $n(t)$ to the received signal $(I_1(t) + s(t))$. Thus, the LNA input is given by

$$r(t) = s(t) + I_1(t) + n(t), \tag{1}$$

where $n(t)$ is composed of the additive noise before the LNA as well as the input referred noise of the LNA and the devices afterwards. For a linear LNA with gain a_1, the LNA output is given by

$$y(t) = a_1 r(t). \tag{2}$$

Then, after the quadrature base-band conversion and sampling, the received signal becomes

$$y_{\rm bb}[k] = a_1 r_{\rm bb}[k] = a_1 \left(s_{\rm bb}[k] + I_{1,\rm bb}[k] + n_{\rm bb}[k]\right). \tag{3}$$

Suppose that the reference receiver provides an estimate of the transmitted interference signal which is input to the interference estimation block at the main receiver whose output is an estimate of the main receiver interference $a_1\hat{I}_{1,\rm bb}[k]$. After the interference estimation, which will be discussed in details in Section III, the cancellation block removes the estimated interference from the received signal, yielding the remaining signal

$$x_{\rm bb}[k] = y_{\rm bb}[k] - a_1\hat{I}_{1,\rm bb}[k] \tag{4}$$

$$= a_1 s_{\rm bb}[k] + \widetilde{n}_{\rm bb}[k] + e[k], \tag{5}$$

where $\widetilde{n}_{\rm bb}[k] = a_1 n_{\rm bb}[k]$ is the noise term and $e[k] = a_1\left(I_{1,\rm bb}[k] - \hat{I}_{1,\rm bb}[k]\right)$ is the residual interference. We call (4) a ''first-order interference removal".

Typically, in order to detect the RAS signal power, the RAS performs a calibration phase to obtain an estimate of the noise power $\hat{P}_{\rm n}$. Then, the RAS signal power is estimated by using the detector in [25] as

$$\hat{P}_{\rm s} = \frac{\overline{|x_{\rm bb}[k]|^2} - \hat{P}_n}{a_1^2}, \tag{6}$$

and we call this detector ''Conventional Detector''. From (5), the time-averaged RAS signal power estimate becomes

$$\overline{|x_{\rm bb}[k]|^2} = a_1^2\overline{|s_{\rm bb}[k]|^2} + \overline{|\widetilde{n}_{\rm bb}[k]|^2} + \Delta \tag{7}$$

where

$$\Delta = \overline{|e[k]|^2} + 2a_1\overline{\Re\{s_{\rm bb}[k]\widetilde{n}^*_{\rm bb}[k]\}} + 2a_1\overline{\Re\{s_{\rm bb}[k]e^*[k]\}} + 2\overline{\Re\{\widetilde{n}_{\rm bb}e^*[k]\}}. \tag{8}$$

Define $P_{\rm n} \triangleq \overline{|\widetilde{n}_{\rm bb}[k]|^2}$, $P_{\rm s} \triangleq \overline{|s_{\rm bb}[k]|^2}$ and $P_{\rm t} \triangleq \overline{|x_{\rm bb}[k]|^2}$. Then, (7) becomes

$$P_{\rm t} = a_1^2 P_{\rm s} + P_{\rm n} + \Delta. \tag{9}$$

By substituting (9) in (6), we obtain

$$\hat{P}_{\rm s} = \frac{P_{\rm t} - \hat{P}_{\rm n}}{a_1^2} = P_{\rm s} + \frac{P_n - \hat{P}_{\rm n}}{a_1^2} + \frac{\Delta}{a_1^2}. \tag{10}$$

Equation (10) shows that the performance of the RAS signal power estimation depends mainly on the RFI cancellation through the third term and on the noise estimation through the second term.

B. RAS SIGNAL POWER ESTIMATION IN A NONLINEAR SYSTEM

In this subsection, we develop a signal model for RAS signal detection when the system behaves nonlinearly, and analyze nonlinearity's effects on the conventional signal detector. In the presence of strong RFI, an LNA would operate in its nolinear region. The typical approximate equation used to define an LNA input-output relation is

$$y(t) = a_1 x(t) + a_3 x^3(t), \tag{11}$$

where we assume a differential output for the LNA, so the second order harmonic is suppressed.

By considering a single tone input signal $x(t) = A\cos(wt)$, the input 1-dB compression point $(A_{\rm 1dB})$ is given by [26]

$$A_{\rm 1dB} = \sqrt{0.145\left|\frac{a_1}{a_3}\right|}. \tag{12}$$

The input 1-dB compression point is defined as the input level at which the gain drops by 1 dB. Throughout this paper we use $a_1 = 1$ and $a_3 = -72.5$ to obtain $P_{\rm 1dB} = \frac{A^2_{\rm 1dB}}{2}$ at 0dBm.

Now, consider the LNA input signal as

$$r(t) = A_1(t)\cos(wt) - A_2(t)\sin(wt) \tag{13}$$

where

$$A_1(t) = \Re\{s_{\rm bb}(t) + I_{1,\rm bb}(t) + n_{\rm bb}(t)\} \tag{14}$$

and

$$A_2(t) = \Im\{s_{\rm bb}(t) + I_{1,\rm bb}(t) + n_{\rm bb}(t)\}. \tag{15}$$

By using (11), the LNA output becomes

$$y(t) = a_1 r(t) + a_3 r^3(t). \tag{16}$$

From (16), the output has two carrier frequencies at w and $3w$, where the latter is removed by filtering since it is located outside the band of interest. Hence, the passband output is given by

$$y(t) = y_{\rm r}(t)\cos(wt) - y_{\rm i}(t)\sin(wt) \tag{17}$$

with

$$y_{\rm r}(t) = a_1 A_1(t) + \frac{3}{4} a_3 \left(A_1^3(t) + A_1(t) A_2^2(t) \right) \tag{18}$$

and

$$y_{\rm i}(t) = a_1 A_2(t) + \frac{3}{4} a_3 \left(A_2^3(t) + A_2(t) A_1^2(t) \right). \tag{19}$$

After down conversion to the baseband and sampling, we get

$$y_{\rm bb}[k] = y_{\rm r}[k] + j\, y_{\rm i}[k]. \tag{20}$$

For notation simplicity, we remove the sampling index. Define $s_{\rm bb} \triangleq s_{\rm r} + j\, s_{\rm i}$, $I_{1,{\rm bb}} \triangleq I_{\rm r} + j I_{\rm i}$ and $n_{\rm bb} \triangleq n_{\rm r} + j\, n_{\rm i}$. Thus, by substituting from (14) and (15) into (18) and (19), we obtain

$$\begin{aligned} y_{\rm r} &= \beta s_{\rm r}^3 + \beta s_{\rm r} s_{\rm i}^2 + 3\beta (n_{\rm r} + I_{\rm r}) s_{\rm r}^2 + \beta (n_{\rm r} + I_{\rm r}) s_{\rm i}^2 \\ &\quad + 2\beta (n_{\rm i} + I_{\rm i}) s_{\rm r} s_{\rm i} + C_1 s_{\rm r} + C_2 s_{\rm i} + C_3^+ \end{aligned} \tag{21}$$

$$\begin{aligned} y_{\rm i} &= \beta s_{\rm i}^3 + \beta s_{\rm i} s_{\rm r}^2 + 3\beta (n_{\rm i} + I_{\rm i}) s_{\rm i}^2 + \beta (n_{\rm i} + I_{\rm i}) s_{\rm r}^2 \\ &\quad + 2\beta (n_{\rm r} + I_{\rm r}) s_{\rm i} s_{\rm r} + D_1 s_{\rm i} + D_2 s_{\rm r} + D_3^+ \end{aligned} \tag{22}$$

where

$$C_1 = \alpha + 3\beta (n_{\rm r} + I_{\rm r})^2 + \beta (n_{\rm i} + I_{\rm i})^2 \tag{23}$$

$$C_2 = 2\beta (n_{\rm i} + I_{\rm i}) (n_{\rm r} + I_{\rm r}) \tag{24}$$

$$C_3^+ = \alpha (n_{\rm r} + I_{\rm r}) + \beta (n_{\rm r} + I_{\rm r})^3 + \beta (n_i + I_{\rm i})^2 (n_{\rm r} + I_{\rm r}) \tag{25}$$

$$D_1 = \alpha + 3\beta (n_{\rm i} + I_{\rm i})^2 + \beta (n_{\rm r} + I_{\rm r})^2 \tag{26}$$

$$D_2 = 2\beta (n_{\rm i} + I_{\rm i}) (n_{\rm r} + I_{\rm r}) \tag{27}$$

$$D_3^+ = \alpha (n_{\rm i} + I_{\rm i}) + \beta (n_{\rm i} + I_{\rm i})^3 + \beta (n_{\rm r} + I_{\rm r})^2 (n_{\rm i} + I_{\rm i}) \tag{28}$$

with $\alpha = a_1$ and $\beta = \frac{3}{4} a_3$. By neglecting $s_{\rm r}^3$, $s_{\rm i}^3$, $s_{\rm r} s_{\rm i}^2$, $s_{\rm i} s_{\rm r}^2$, $s_{\rm r}^2$, $s_{\rm i}^2$ and $s_{\rm i} s_{\rm r}$, since they are insignificant compared to other terms, (21) and (22) are approximated as

$$y_{\rm r} \simeq C_1 s_{\rm r} + C_2 s_{\rm i} + C_3^+ \tag{29}$$

and

$$y_{\rm i} \simeq D_1 s_{\rm i} + D_2 s_{\rm r} + D_3^+. \tag{30}$$

By expanding C_3^+ and D_3^+ , we get

$$\begin{aligned} C_3^+ &= \beta n_{\rm r}^3 + 3\beta I_{\rm r} n_{\rm r}^2 + \left(\alpha + \beta \left(3I_{\rm r}^2 + I_{\rm i}^2 \right) \right) n_{\rm r} + 2\beta I_{\rm i} n_{\rm i} n_{\rm r} \\ &\quad + \beta n_{\rm i}^2 n_{\rm r} + \beta I_{\rm r} n_{\rm i}^2 + 2\beta I_{\rm r} I_{\rm i} n_{\rm i} + \alpha I_{\rm r} + \beta I_{\rm r}^3 + \beta I_{\rm r} I_{\rm i}^2 \end{aligned} \tag{31}$$

$$\begin{aligned} D_3^+ &= \beta n_{\rm i}^3 + 3\beta I_{\rm i} n_{\rm i}^2 + \left(\alpha + \beta \left(3I_{\rm i}^2 + I_{\rm r}^2 \right) \right) n_{\rm i} + 2\beta I_{\rm r} n_{\rm r} n_{\rm i} \\ &\quad + \beta n_{\rm r}^2 n_{\rm i} + \beta I_{\rm i} n_{\rm r}^2 + 2\beta I_{\rm i} I_{\rm r} n_{\rm r} + \alpha I_{\rm i} + \beta I_{\rm i}^3 + \beta I_{\rm i} I_{\rm r}^2. \end{aligned} \tag{32}$$

It is noticed from (31) that most of the interference terms are multiplied by noise terms. Thus, it is impossible to eliminate them instantaneously except the three terms $\alpha I_{\rm r}$, $\beta I_{\rm r}^3$ and $\beta I_{\rm r} I_{\rm i}^2$, which we can estimate and remove instantaneously. Similarly, in (32) we can estimate the terms $\alpha I_{\rm i}$, $\beta I_{\rm i}^3$ and $\beta I_{\rm i} I_{\rm r}^2$, and then remove them instantaneously. By removing the estimates of these terms from (29) and (30), the real and imaginary parts of the remaining signal are defined as

$$z_{\rm r} \triangleq y_{\rm r} - \left(\alpha \hat{I}_{\rm r} + \beta \hat{I}_{\rm r}^3 + \beta \hat{I}_{\rm r} \hat{I}_{\rm i}^2 \right) \tag{33}$$

$$= C_1 s_{\rm r} + C_2 s_{\rm i} + C_3 + \xi_{\rm r,res} \tag{34}$$

and

$$z_{\rm i} \triangleq y_{\rm i} - \left(\alpha \hat{I}_{\rm i} + \beta \hat{I}_{\rm i}^3 + \beta \hat{I}_{\rm i} \hat{I}_{\rm r}^2 \right) \tag{35}$$

$$= D_1 s_{\rm i} + D_2 s_{\rm r} + D_3 + \xi_{\rm i,res} \tag{36}$$

where

$$C_3 = C_3^+ - \left(\alpha I_{\rm r} + \beta I_{\rm r}^3 + \beta I_{\rm r} I_{\rm i}^2 \right) \tag{37}$$

$$\begin{aligned} &= \beta n_{\rm r}^3 + 3\beta I_{\rm r} n_{\rm r}^2 + \beta n_{\rm i}^2 n_{\rm r} + \left(\alpha + \beta \left(3I_{\rm r}^2 + I_{\rm i}^2 \right) \right) n_{\rm r} \\ &\quad + 2\beta I_{\rm i} n_{\rm i} n_{\rm r} + \beta I_{\rm r} n_{\rm i}^2 + 2\beta I_{\rm r} I_{\rm i} n_{\rm i} \end{aligned} \tag{38}$$

$$D_3 = D_3^+ - \left(\alpha I_{\rm i} + \beta I_{\rm i}^3 + \beta I_{\rm i} I_{\rm r}^2 \right) \tag{39}$$

$$\begin{aligned} &= \beta n_{\rm i}^3 + 3\beta I_{\rm i} n_{\rm i}^2 + \beta n_{\rm r}^2 n_{\rm i} + \left(\alpha + \beta \left(3I_{\rm i}^2 + I_{\rm r}^2 \right) \right) n_{\rm i} \\ &\quad + 2\beta I_{\rm r} n_{\rm r} n_{\rm i} + \beta I_{\rm i} n_{\rm r}^2 + 2\beta I_{\rm i} I_{\rm r} n_{\rm r} \end{aligned} \tag{40}$$

$$\xi_{\rm r,res} = \alpha \left(I_{\rm r} - \hat{I}_{\rm r} \right) + \beta \left(I_{\rm r}^3 - \hat{I}_{\rm r}^3 \right) + \beta \left(I_{\rm r} I_{\rm i}^2 - \hat{I}_{\rm r} \hat{I}_{\rm i}^2 \right) \tag{41}$$

$$\xi_{\rm i,res} = \alpha \left(I_{\rm i} - \hat{I}_{\rm i} \right) + \beta \left(I_{\rm i}^3 - \hat{I}_{\rm i}^3 \right) + \beta \left(I_{\rm i} I_{\rm r}^2 - \hat{I}_{\rm i} \hat{I}_{\rm r}^2 \right). \tag{42}$$

We call this kind of interference removal "higher order interference removal". To proceed, we need to calculate $\overline{z_{\rm r}^2}$ and $\overline{z_{\rm i}^2}$. By squaring (34) and (36), we obtain

$$\begin{aligned} z_{\rm r}^2 &= C_1^2 s_{\rm r}^2 + C_2^2 s_{\rm i}^2 + C_3^2 + \xi_{\rm r,res}^2 + 2C_1 C_2 s_{\rm r} s_{\rm i} + 2C_1 C_3 s_{\rm r} \\ &\quad + 2C_2 C_3 s_{\rm i} + \xi_{\rm r,res} \left(C_1 s_{\rm r} + C_2 s_{\rm i} + C_3 \right) \end{aligned} \tag{43}$$

and

$$\begin{aligned} z_{\rm i}^2 &= D_1^2 s_{\rm i}^2 + D_2^2 s_{\rm r}^2 + D_3^2 + \xi_{\rm i,res}^2 + 2D_1 D_2 s_{\rm i} s_{\rm r} + 2D_1 D_3 s_{\rm i} \\ &\quad + 2D_2 D_3 s_{\rm r} + \xi_{\rm i,res} \left(D_1 s_{\rm i} + D_2 s_{\rm r} + D_3 \right). \end{aligned} \tag{44}$$

Then, by averaging over m samples, we obtain

$$\overline{z_{\rm r}^2} = \overline{C_1^2}\, \overline{s_{\rm r}^2} + \overline{C_2^2}\, \overline{s_{\rm i}^2} + \overline{C_3^2} + \overline{\xi_{\rm r,res}^2} + \zeta_{\rm r,res} \tag{45}$$

$$\overline{z_{\rm i}^2} = \overline{D_1^2}\, \overline{s_{\rm i}^2} + \overline{D_2^2}\, \overline{s_{\rm r}^2} + \overline{D_3^2} + \overline{\xi_{\rm i,res}^2} + \zeta_{\rm i,res} \tag{46}$$

where $\zeta_{\rm r,res}$ and $\zeta_{\rm i,res}$ are the residual errors due to the finite sum of $z_{\rm r}^2$ and $z_{\rm i}^2$ samples respectively. Next, from (23), (26), (24), (27), (38) and (40), we obtain the following terms:

$$\begin{aligned} \overline{C_1^2} &= \alpha^2 + 9\beta^2 \overline{I_{\rm r}^4} + \beta^2 \overline{I_{\rm i}^4} + \left(54\beta^2 \overline{n_{\rm r}^2} + 6\alpha\beta + 6\beta^2 \overline{n_{\rm i}^2} \right) \overline{I_{\rm r}^2} \\ &\quad + \left(6\beta^2 \overline{n_{\rm r}^2} + 2\alpha\beta + 6\beta^2 \overline{n_{\rm i}^2} \right) \overline{I_{\rm i}^2} + 6\beta^2 \overline{I_{\rm r}^2 I_{\rm i}^2} \\ &\quad + 9\beta^2 \overline{n_{\rm r}^4} + \beta^2 \overline{n_{\rm i}^4} + 6\alpha\beta \overline{n_{\rm r}^2} + 2\alpha\beta \overline{n_{\rm i}^2} + 6\beta^2 \overline{n_{\rm r}^2 n_{\rm i}^2} \end{aligned} \tag{47}$$

$$\begin{aligned} \overline{D_1^2} &= \alpha^2 + 9\beta^2 \overline{I_{\rm i}^4} + \beta^2 \overline{I_{\rm r}^4} + \left(54\beta^2 \overline{n_{\rm i}^2} + 6\alpha\beta + 6\beta^2 \overline{n_{\rm r}^2} \right) \overline{I_{\rm i}^2} \\ &\quad + \left(6\beta^2 \overline{n_{\rm i}^2} + 2\alpha\beta + 6\beta^2 \overline{n_{\rm r}^2} \right) \overline{I_{\rm r}^2} + 6\beta^2 \overline{I_{\rm r}^2 I_{\rm i}^2} \\ &\quad + 9\beta^2 \overline{n_{\rm i}^4} + \beta^2 \overline{n_{\rm r}^4} + 6\alpha\beta \overline{n_{\rm i}^2} + 2\alpha\beta \overline{n_{\rm r}^2} + 6\beta^2 \overline{n_{\rm r}^2 n_{\rm i}^2} \end{aligned} \tag{48}$$

$$\overline{C_2^2} = 4\beta^2\overline{n_{\rm i}^2}\overline{n_{\rm r}^2} + 4\beta^2\overline{n_{\rm i}^2}\overline{I_{\rm r}^2} + 4\beta^2\overline{n_{\rm r}^2}\overline{I_{\rm i}^2} + 4\beta^2\overline{I_{\rm r}^2}\overline{I_{\rm i}^2} \quad (49)$$

$$\overline{D_2^2} = 4\beta^2\overline{n_{\rm i}^2}\overline{n_{\rm r}^2} + 4\beta^2\overline{n_{\rm i}^2}\overline{I_{\rm r}^2} + 4\beta^2\overline{n_{\rm r}^2}\overline{I_{\rm i}^2} + 4\beta^2\overline{I_{\rm r}^2}\overline{I_{\rm i}^2} \quad (50)$$

$$\begin{aligned}\overline{C_3^2} = {} & \left(9\beta^2\overline{n_{\rm r}^2}\right)\overline{I_{\rm r}^4} + \left(\beta^2\overline{n_{\rm r}^2}\right)\overline{I_{\rm i}^4} + \left(6\beta^2\overline{n_{\rm r}^2} + 4\beta^2\overline{n_{\rm i}^2}\right)\overline{I_{\rm r}^2 I_{\rm i}^2} \\ & + \left(6\alpha\beta\overline{n_{\rm r}^2} + 15\beta^2\overline{n_{\rm r}^4} + 12\beta^2\overline{n_{\rm r}^2 n_{\rm i}^2} + \beta^2\overline{n_{\rm i}^4}\right)\overline{I_{\rm r}^2} \\ & + \left(2\alpha\beta\overline{n_{\rm r}^2} + 2\beta^2\overline{n_{\rm r}^4} + 6\beta^2\overline{n_{\rm r}^2 n_{\rm i}^2}\right)\overline{I_{\rm i}^2} + \alpha^2\overline{n_{\rm r}^2} \\ & + 2\alpha\beta\overline{n_{\rm r}^4} + 2\alpha\beta\overline{n_{\rm r}^2 n_{\rm i}^2} + \beta^2\overline{n_{\rm r}^6} + 2\beta^2\overline{n_{\rm r}^4 n_{\rm i}^2} + \beta^2\overline{n_{\rm r}^2 n_{\rm i}^4}\end{aligned} \quad (51)$$

$$\begin{aligned}\overline{D_3^2} = {} & \left(9\beta^2\overline{n_{\rm i}^2}\right)\overline{I_{\rm i}^4} + \left(\beta^2\overline{n_{\rm i}^2}\right)\overline{I_{\rm r}^4} + \left(6\beta^2\overline{n_{\rm i}^2} + 4\beta^2\overline{n_{\rm r}^2}\right)\overline{I_{\rm r}^2 I_{\rm i}^2} \\ & + \left(6\alpha\beta\overline{n_{\rm i}^2} + 15\beta^2\overline{n_{\rm i}^4} + 12\beta^2\overline{n_{\rm r}^2 n_{\rm i}^2} + \beta^2\overline{n_{\rm r}^4}\right)\overline{I_{\rm i}^2} \\ & + \left(2\alpha\beta\overline{n_{\rm i}^2} + 2\beta^2\overline{n_{\rm i}^4} + 6\beta^2\overline{n_{\rm r}^2 n_{\rm i}^2}\right)\overline{I_{\rm r}^2} + \alpha^2\overline{n_{\rm i}^2} \\ & + 2\alpha\beta\overline{n_{\rm i}^4} + 2\alpha\beta\overline{n_{\rm r}^2 n_{\rm i}^2} + \beta^2\overline{n_{\rm i}^6} + 2\beta^2\overline{n_{\rm i}^4 n_{\rm r}^2} + \beta^2\overline{n_{\rm i}^2 n_{\rm r}^4}.\end{aligned} \quad (52)$$

Note that the errors due to the finite averaging window in $\overline{C_1^2}$, $\overline{C_2^2}$, $\overline{C_3^2}$, $\overline{D_1^2}$, $\overline{D_2^2}$ and $\overline{D_3^2}$ are included in $\zeta_{\rm r,res}$ and $\zeta_{\rm i,res}$. Now, by using the "Conventional Detector" given in (6), we show the effect of nonlinearity on the performance of the RAS signal power estimation. For simplicity, for this part only, we assume the following:

1) The received interference at the main receiver is estimated perfectly (i.e, $\hat{I}_{\rm r} = I_{\rm r}$ and $\hat{I}_{\rm i} = I_{\rm i}$), thus $\xi_{\rm r,res} = \xi_{\rm i,res} = 0$.
2) The averaging process is done over a very large number of samples. Hence, $\overline{I_{\rm r}^2} = \overline{I_{\rm i}^2}$, $\overline{I_{\rm r}^4} = \overline{I_{\rm i}^4}$, $\overline{n_{\rm r}^2} = \overline{n_{\rm i}^2} = \sigma_{\rm n}^2$, $\overline{n_{\rm r}^4} = \overline{n_{\rm i}^4} = 3\sigma_{\rm n}^4$, $\overline{n_{\rm r}^6} = \overline{n_{\rm i}^6} = 15\sigma_{\rm n}^6$, $\overline{s_{\rm r}^2} = \overline{s_{\rm i}^2} = \sigma_s^2$, and $\zeta_{\rm r,res} = \zeta_{\rm i,res} = 0$.

Using these assumptions, we find that $\overline{C_1^2} = \overline{D_1^2}$, $\overline{C_2^2} = \overline{D_2^2}$ and $\overline{C_3^2} = \overline{D_3^2}$. Defining $C \triangleq \overline{C_1^2} + \overline{C_2^2} \simeq \frac{\overline{C_3^2}}{\sigma_{\rm n}^2}$, we obtain

$$\overline{z_{\rm r}^2} = \overline{z_{\rm i}^2} = C(\sigma_s^2 + \sigma_{\rm n}^2). \quad (53)$$

By using the "Conventional Detector" given in (6), we obtain the RAS signal power estimate as

$$\hat{P}_{\rm s} = \frac{2\overline{z_{\rm r}^2} - 2\sigma_{\rm n}^2}{a_1^2}. \quad (54)$$

We define the absolute normalized error in the RAS signal power detection as

$$e_{\rm norm} \triangleq \left|\frac{\hat{P}_{\rm s} - P_{\rm s}}{P_{\rm s}}\right|. \quad (55)$$

Thus, by substituting (53) into (55), we obtain

$$e_{\rm norm} = \frac{|C-1|\left(\sigma_s^2 + \sigma_n^2\right)}{\sigma_s^2}. \quad (56)$$

Due to the two assumptions mentioned above, (56) leaves out the contributions from interference estimation and time averaging and shows the error performance of the conventional detector caused by nonlinearity only. We plot (56) in Fig. 2 to show the effect of nonlinearity on the conventional detector with higher order interference cancellation. It is obvious that when the interference level increases the absolute normalized error ($e_{\rm norm}$) increases significantly, and becomes even worse when the RAS signal level decreases.

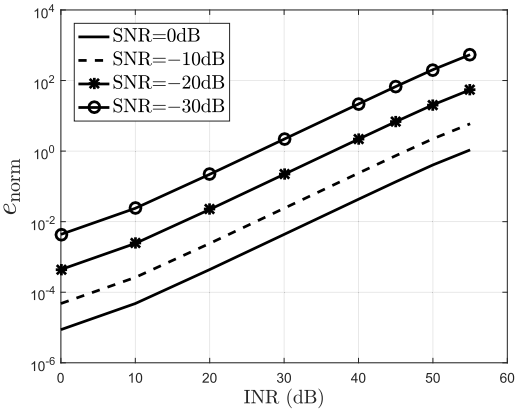

FIGURE 2. Plot of (56) that shows the effect of the system nonlinearity on the RAS signal detection.

III. A NEW DETECTOR UNDER NONLINEAR RFI

In the last section, we showed that the conventional detector fails when the LNA operates in a nonlinear region. This failure occurs as the conventional detector does not consider the system nonlinearity. In this section, we propose a new detector based on the signal model that captures the effects of an LNA nonlinearity on the received signal, which is derived in the last section. From (45) and (46) and by defining $\Xi_{\rm r} \triangleq \overline{\xi_{\rm r,res}^2} + \zeta_{\rm r,res}$ and $\Xi_{\rm i} \triangleq \overline{\xi_{\rm i,res}^2} + \zeta_{\rm i,res}$, we can write a new signal model for RAS signal detection as

$$\underbrace{\begin{bmatrix}\overline{z_{\rm r}^2}\\ \overline{z_{\rm i}^2}\end{bmatrix}}_{\mathbf{z}\in\mathbb{R}^{2\times1}} = \underbrace{\begin{bmatrix}\overline{C_1^2} & \overline{C_2^2}\\ \overline{D_2^2} & \overline{D_1^2}\end{bmatrix}}_{\mathbf{G}\in\mathbb{R}^{2\times2}} \underbrace{\begin{bmatrix}\overline{s_{\rm r}^2}\\ \overline{s_{\rm i}^2}\end{bmatrix}}_{\mathbf{p}\in\mathbb{R}^{2\times1}} + \underbrace{\begin{bmatrix}\overline{C_3^2}\\ \overline{D_3^2}\end{bmatrix}}_{\mathbf{n}_{\rm new}\in\mathbb{R}^{2\times1}} + \underbrace{\begin{bmatrix}\Xi_{\rm r}\\ \Xi_{\rm i}\end{bmatrix}}_{\Xi\in\mathbb{R}^{2\times1}}. \quad (57)$$

Then, we can obtain the least square estimate of $\mathbf{p}$ as

$$\hat{\mathbf{p}} = \hat{\mathbf{G}}^{-1}\left(\mathbf{z} - \hat{\mathbf{n}}_{\rm new}\right), \quad (58)$$

and then the RAS signal power as

$$\hat{P}_s = [1,\ 1]\,\hat{\mathbf{p}}. \quad (59)$$

The superiority of this detector over the conventional one in (6) is established through its ability to incorporate nonlinearity-induced terms.

To reduce the RAS detection error ($e_{\rm norm}$), we need reliable estimates $\hat{\mathbf{G}}$ and $\hat{\mathbf{n}}_{\rm new}$ which in turn require good estimates of $\overline{C_1^2}$, $\overline{C_2^2}$, $\overline{C_3^2}$, $\overline{D_1^2}$, $\overline{D_2^2}$ and $\overline{D_3^2}$. Furthermore, Ξ should be suppressed too. These can be accomplished by a good system calibration to deduce the noise power correctly, an averaging process over a large window of samples, and a reliable interference estimation. Throughout this paper, we assume a perfect estimation of the noise power (i.e., $\hat{P}_n = P_n$). Hence, to

obtain good signal detection performance, our focus is to estimate the interference reliably.

Consider the received interference sample at time k at the reference antenna given by

$$I_{2,\mathrm{bb}}[k] = \mathbf{u}_{\mathrm{ref}}^T[k]\mathbf{h}_{\mathrm{ref}} \tag{60}$$

where

$$\mathbf{h}_{\mathrm{ref}} = [h_{0,\mathrm{ref}}, h_{1,\mathrm{ref}}, \ldots, h_{L_{\mathrm{ref}}-1,\mathrm{ref}}]^T \in \mathbb{C}^{L_{\mathrm{ref}}\times 1} \tag{61}$$

is the channel impulse response (CIR) for the reference receiver and

$$\mathbf{u}_{\mathrm{ref}}[k] = [u[k], u[k-1], \ldots, u[k-L_{\mathrm{ref}}+1]]^T \in \mathbb{C}^{L_{\mathrm{ref}}\times 1} \tag{62}$$

is a vector that contains the transmitted samples of the CWC. Similarly, the received interference sample at time k at the main receiver antenna is

$$I_{1,\mathrm{bb}}[k] = \mathbf{u}^T[k]\mathbf{h} \tag{63}$$

where

$$\mathbf{h} = [h_0, h_1, \ldots, h_{L-1}]^T \in \mathbb{C}^{L\times 1} \tag{64}$$

is the CIR for the main receiver and

$$\mathbf{u}[k] = [u[k], u[k-1], \ldots, u[k-L+1]]^T \in \mathbb{C}^{L\times 1} \tag{65}$$

is a vector that contains the transmitted samples of the CWC.

In this paper, we assume that $\{u[k]\}$ are detected correctly at the reference receiver and then passed to the main receiver. Accordingly, our objective is to perform a reliable estimation of the channel for the main receiver so that accurate interference signal can be reconstructed for RFI cancellation. In this section, we present two methods to estimate the main receiver channel when the system operates in a nonlinear region. In the first method, we use a modified Kalman filter called the "Unscented Kalman Filter" (UKF) [21]–[23] that performs well with nonlinear systems. In the second method, we propose a new approach based on a nonlinear-to-linear mapping.

A. UNSCENTED KALMAN FILTER-BASED CHANNEL ESTIMATION

Kalman filter [27] is an iterative minimum mean square error filter used to estimate the states of a linear system. To cope with nonlinear systems, Julier *et al.* [21]–[23] introduced the unscented Kalman filter. The nonlinear state space model of a system that the UKF operates on is given in [28] as

$$\mathbf{x}[k] = \mathbf{f}_1(\mathbf{x}[k-1], k) + \boldsymbol{\omega}[k] \tag{66}$$

$$\boldsymbol{\theta}[k] = \mathbf{g}(\mathbf{x}[k], k) + \boldsymbol{\nu}_{\mathrm{n}}[k], \tag{67}$$

where (66) and (67) are called the state equation and the output equation respectively. $\mathbf{x}[k] \in \mathbb{R}^{n_1\times 1}$, $\boldsymbol{\theta}[k] \in \mathbb{R}^{n_2\times 1}$, $\boldsymbol{\omega}[k] \in \mathbb{R}^{n_1\times 1}$ and $\boldsymbol{\nu}_{\mathrm{n}}[k] \in \mathbb{R}^{n_2\times 1}$ are the states vector, the outputs vector, the states noise vector and the outputs noise vector, respectively, at time k. $\mathbf{f}_1(\cdot) : \mathbb{R}^{n\times 1} \to \mathbb{R}^{n\times 1}$ and $\mathbf{g}(\cdot) : \mathbb{R}^{n\times 1} \to \mathbb{R}^{m\times 1}$ are generally nonlinear and time-variant functions.

For our system, we define a state space model with states that depend on the channel taps values, and outputs that are related to the LNA outputs. Accordingly, (63) is reorganized as

$$I_{1,\mathrm{bb}}[k] = \underbrace{\mathbf{v}^T(k)\,\mathbf{h}_{\mathrm{new}}}_{I_{\mathrm{r}}[k]} + j\underbrace{\mathbf{w}^T(k)\,\mathbf{h}_{\mathrm{new}}}_{I_{\mathrm{i}}[k]} \tag{68}$$

where (69)–(71) are shown at the bottom of this page and $N = 2L$. By omitting the insignificant terms from (21) and (22) and substituting (68) into them, we approximate the real and imaginary parts of the lowpass-equivalent LNA outputs as

$$y_{\mathrm{r}}[k] \simeq \alpha I_{\mathrm{r}}[k] + \beta\left(I_{\mathrm{r}}^3[k] + I_{\mathrm{r}}[k]I_{\mathrm{i}}^2[k]\right) + n_{\mathrm{r}}[k] \tag{72}$$

$$= \alpha\mathbf{v}^T[k]\mathbf{h}_{\mathrm{new}} + \beta\left(\mathbf{v}^T[k]\mathbf{h}_{\mathrm{new}}\right)^3 + \beta\left(\left(\mathbf{v}^T[k]\mathbf{h}_{\mathrm{new}}\right)\left(\mathbf{w}^T[k]\mathbf{h}_{\mathrm{new}}\right)^2\right) + n_{\mathrm{r}}(k) \tag{73}$$

$$y_{\mathrm{i}}[k] \simeq \alpha I_{\mathrm{i}}[k] + \beta\left(I_{\mathrm{i}}^3[k] + I_{\mathrm{i}}[k]I_{\mathrm{r}}^2[k]\right) + n_{\mathrm{i}}[k] \tag{74}$$

$$= \alpha\mathbf{w}^T[k]\mathbf{h}_{\mathrm{new}} + \beta\left(\mathbf{w}^T[k]\mathbf{h}_{\mathrm{new}}\right)^3 + \beta\left(\left(\mathbf{w}^T[k]\mathbf{h}_{\mathrm{new}}\right)\left(\mathbf{v}^T[k]\mathbf{h}_{\mathrm{new}}\right)^2\right) + n_{\mathrm{i}}[k]. \tag{75}$$

Since our purpose is to estimate the channel taps, now given in $\mathbf{h}_{\mathrm{new}}$, we consider the states as

$$\mathbf{x}[k] = \mathbf{h}_{\mathrm{new}}. \tag{76}$$

In addition, the model outputs are assigned as

$$\theta_1[k] = y_{\mathrm{r}}[k] \tag{77}$$

$$\theta_2[k] = y_{\mathrm{i}}[k]. \tag{78}$$

Since $\mathbf{h}_{\mathrm{new}}$ is fixed over the period that we estimate on, the states equation becomes

$$\mathbf{x}[k] = \mathbf{x}[k-1]. \tag{79}$$

By substituting (76) into (73) and (75), we obtain the output equations as

$$\theta_1[k] = g_1(\mathbf{x}[k]) + n_{\mathrm{r}}[k] \tag{80}$$

$$\theta_2[k] = g_2(\mathbf{x}[k]) + n_{\mathrm{i}}[k] \tag{81}$$

$$\mathbf{v}[k] = \begin{bmatrix} u_{\mathrm{r}}[k] & -u_{\mathrm{i}}[k] & u_{\mathrm{r}}[k-1] & -u_{\mathrm{i}}[k-1] & \cdots & u_{\mathrm{r}}[k-L+1] & -u_{\mathrm{i}}[k-L+1] \end{bmatrix}^T \in \mathbb{R}^{N\times 1} \tag{69}$$

$$\mathbf{w}[k] = \begin{bmatrix} u_{\mathrm{i}}[k] & u_{\mathrm{r}}[k] & u_{\mathrm{i}}[k-1] & u_{\mathrm{r}}[k-1] & \cdots & u_{\mathrm{i}}[k-L+1] & u_{\mathrm{r}}[k-L+1] \end{bmatrix}^T \in \mathbb{R}^{N\times 1} \tag{70}$$

$$\mathbf{h}_{\mathrm{new}} = \begin{bmatrix} h_{\mathrm{r},0} & h_{\mathrm{i},0} & \cdots & h_{\mathrm{r},L-1} & h_{\mathrm{i},L-1} \end{bmatrix}^T \in \mathbb{R}^{N\times 1} \tag{71}$$

$$\boldsymbol{\chi}_i[k-1|k-1] = \begin{cases} \hat{\mathbf{x}}[k-1|k-1] & i=0 \\ \hat{\mathbf{x}}[k-1|k-1] + \left(\sqrt{\frac{N}{1-w_{\mathrm{m}}(0)}}\mathbf{P}_{\mathbf{xx}}^{\frac{1}{2}}[k-1|k-1]\right)_i & 1 \le i \le N \\ \hat{\mathbf{x}}[k-1|k-1] - \left(\sqrt{\frac{N}{1-w_{\mathrm{m}}(0)}}\mathbf{P}_{\mathbf{xx}}^{\frac{1}{2}}[k-1|k-1]\right)_{i-N} & N+1 \le i \le 2N \end{cases} \tag{85}$$

where

$$g_1(\mathbf{x}[k]) = \alpha \mathbf{v}^T[k]\mathbf{x}[k] + \beta\left(\mathbf{v}^T[k]\mathbf{x}[k]\right)^3 + \beta\left(\left(\mathbf{v}^T[k]\mathbf{x}[k]\right)\left(\mathbf{w}^T[k]\mathbf{x}[k]\right)^2\right) \tag{82}$$

$$g_2(\mathbf{x}[k]) = \alpha \mathbf{w}^T[k]\mathbf{x}[k] + \beta\left(\mathbf{w}^T[k]\mathbf{x}[k]\right)^3 + \beta\left(\left(\mathbf{w}^T[k]\mathbf{x}[k]\right)\left(\mathbf{v}^T[k]\mathbf{x}[k]\right)^2\right) \tag{83}$$

and we can write these equations as

$$\underbrace{\begin{bmatrix}\theta_1[k]\\ \theta_2[k]\end{bmatrix}}_{\boldsymbol{\theta}[k]} = \underbrace{\begin{bmatrix}g_1(\mathbf{x}[k])\\ g_2(\mathbf{x}[k])\end{bmatrix}}_{\mathbf{g}(\mathbf{x}[k])} + \underbrace{\begin{bmatrix}n_{\mathrm{r}}[k]\\ n_{\mathrm{i}}[k]\end{bmatrix}}_{\boldsymbol{\nu}_{\mathrm{n}}[k]}. \tag{84}$$

Now, after defining the state space model, we perform an UKF algorithm described as follows:

i) Obtain $(2N+1)$ points as in (85) (shown at the top of this page), where $(\,)_i$ represents the ith column vector of the matrix inside the bracket. The samples ($\boldsymbol{\chi}_i[k-1|k-1] \in \mathbb{R}^{N\times 1}$) have a mean of $\hat{\mathbf{x}}[k-1|k-1] \in \mathbb{R}^{N\times 1}$ and a covariance matrix $\mathbf{P}_{\mathbf{xx}}[k-1|k-1] \in \mathbb{R}^{N\times N}$.

ii) Update those samples using the state equation in (79) on the samples to obtain

$$\boldsymbol{\chi}_i[k|k-1] = \boldsymbol{\chi}_i[k-1|k-1] \tag{86}$$

with the estimated mean

$$\hat{\mathbf{x}}[k|k-1] = \sum_{i=0}^{2N} w_{\mathrm{m}}(i)\boldsymbol{\chi}_i[k|k-1] \tag{87}$$

and the estimated covariance matrix

$$\mathbf{P}_{\mathbf{xx}}[k|k-1] = \sum_{i=0}^{2N}\left(w_{\mathrm{c}}(i)\left[\boldsymbol{\chi}_i[k|k-1] - \hat{\mathbf{x}}[k|k-1]\right] \times \left[\boldsymbol{\chi}_i[k|k-1] - \hat{\mathbf{x}}[k|k-1]\right]^{\mathrm{T}}\right) \tag{88}$$

where $w_{\mathrm{m}}(i) = w_{\mathrm{c}}(i) = \frac{1-w_{\mathrm{m}}(0)}{2N}$ for $i \neq 0$ and $w_{\mathrm{c}}(0) = w_{\mathrm{m}}(0) + \left(1 - c^2 + \epsilon\right)$. Note that c^2, $w_{\mathrm{m}}(0)$ and ϵ are constants and they are adjusted as in [23].

iii) Apply the output equation (84) on the samples to get the estimated samples of observations given by

$$\boldsymbol{\psi}_i[k|k-1] = \mathbf{g}\left(\boldsymbol{\chi}_i[k|k-1]\right) \in \mathbb{R}^{2\times 1} \tag{89}$$

with the estimated mean

$$\hat{\boldsymbol{\theta}}[k|k-1] = \sum_{i=0}^{2N} w_{\mathrm{m}}(i)\boldsymbol{\psi}_i[k|k-1] \in \mathbb{R}^{2\times 1}. \tag{90}$$

iv) Calculate the estimated cross-covariance matrix of the states and the observations as

$$\mathbf{P}_{\mathbf{x}\boldsymbol{\theta}}[k|k-1] = \sum_{i=0}^{2N}\left(w_{\mathrm{c}}(i)\left[\boldsymbol{\chi}_i[k|k-1] - \hat{\mathbf{x}}[k|k-1]\right] \times \left[\boldsymbol{\psi}_i[k|k-1] - \hat{\boldsymbol{\theta}}[k|k-1]\right]^{\mathrm{T}}\right) \in \mathbb{R}^{N\times 2}. \tag{91}$$

v) Define the error between the actual observation and the estimated one as $\boldsymbol{\nu}[k] \triangleq \boldsymbol{\theta}(k) - \hat{\boldsymbol{\theta}}[k|k-1]$ and compute its covariance matrix $\mathbf{P}_{\boldsymbol{\nu}\boldsymbol{\nu}}[k|k-1] \in \mathbb{R}^{2\times 2}$ as

$$\mathbf{P}_{\boldsymbol{\nu}\boldsymbol{\nu}}[k|k-1] = \sum_{i=0}^{2N}\left(w_{\mathrm{c}}(i)\left[\boldsymbol{\psi}_i[k|k-1] - \hat{\boldsymbol{\theta}}[k|k-1]\right] \times \left[\boldsymbol{\psi}_i[k|k-1] - \hat{\boldsymbol{\theta}}[k|k-1]\right]^{\mathrm{T}}\right) + \mathbf{R}_{\mathrm{n}} \tag{92}$$

where $\mathbf{R}_n \in \mathbb{R}^{2\times 2}$ is the covariance matrix of $\boldsymbol{\nu}_{\mathrm{n}}[k]$.

vi) Compute the Kalman filter gain to filter the estimated states vector as

$$\mathbf{K}[k] = \mathbf{P}_{\mathbf{x}\boldsymbol{\theta}}[k|k-1]\mathbf{P}_{\boldsymbol{\nu}\boldsymbol{\nu}}^{-1}[k|k-1] \in \mathbb{R}^{N\times 2}. \tag{93}$$

vii) Update the states mean and the states covariance matrix as

$$\hat{\mathbf{x}}[k|k] = \hat{\mathbf{x}}[k|k-1] + \mathbf{K}[k]\boldsymbol{\nu}[k] \tag{94}$$

$$\mathbf{P}_{\mathbf{xx}}[k|k] = \mathbf{P}_{\mathbf{xx}}[k|k-1] - \mathbf{K}[k]\mathbf{P}_{\mathbf{x}\boldsymbol{\theta}}^T[k|k-1]. \tag{95}$$

After applying that filter on μ samples, we obtain an estimate $\hat{\mathbf{h}}_{\mathrm{new}}$ as

$$\hat{\mathbf{h}}_{\mathrm{new}} = \hat{\mathbf{x}}[\mu|\mu]. \tag{96}$$

Then, the estimated interference at the main receiver at time k is constructed as

$$\hat{I}_{1,\mathrm{bb}}[k] = \underbrace{\mathbf{v}^T(k)\hat{\mathbf{h}}_{\mathrm{new}}}_{\hat{I}_{\mathrm{r}}[k]} + j\underbrace{\mathbf{w}^T(k)\hat{\mathbf{h}}_{\mathrm{new}}}_{\hat{I}_{\mathrm{i}}[k]}. \tag{97}$$

Note that at the beginning of the UKF algorithm, we need initial estimates for the states mean vector $\mathbf{x}(0|0)$ and the states covariance matrix $\mathbf{P}_{\mathbf{xx}}(0|0)$. In particular, a good initial value of $\mathbf{x}(0|0)$ is needed, otherwise the state estimation at high interference power will diverge from the optimal solution. We will discuss how to obtain this initial value $\mathbf{x}(0|0) = \hat{\mathbf{h}}_{\mathrm{new,int}}$ later in this section.

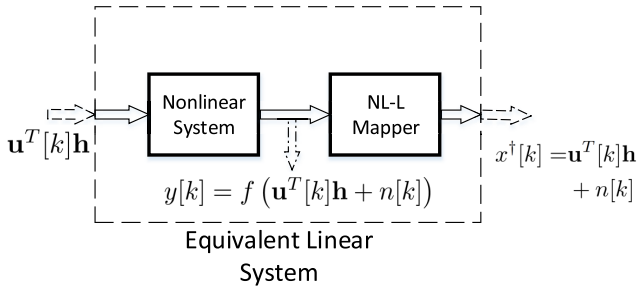

FIGURE 3. The proposed nonlinear to linear mapping approach.

B. NONLINEAR TO LINEAR MAPPING METHOD

In this subsection, we propose a new method to estimate the channel in a nonlinear system. We propose a nonlinear mapper that maps the LNA output, which depends nonlinearly on the channel, into a linear output that depends linearly on the channel. This means that the LNA together with the mapper act equivalently as a linear system as in Fig. 3. After we implement that equivalent system, it becomes straightforward to estimate the channel using a least square method. The mapping process is done in two stages. The first stage determines all the possible solutions for the LNA nonlinear output. The second stage decides for each sample which solution is the best choice. To implement the first stage, we consider the LNA output from the last section and we neglect the RAS signal as it is insignificant. Then by substituting (14) and (15) in (18) and (19), the real and imaginary parts of the lowpass-equivalent LNA output at time k become

$$\begin{aligned} y_{\mathrm{r}}[k] &= \alpha\left(I_{\mathrm{r}}[k] + n_{\mathrm{r}}[k]\right) + \beta\left(I_{\mathrm{r}}[k] + n_{\mathrm{r}}[k]\right)^3 \\ &\quad + \beta\left(I_{\mathrm{r}}[k] + n_{\mathrm{r}}[k]\right)\left(I_{\mathrm{i}}[k] + n_{\mathrm{i}}[k]\right)^2 \qquad (98) \\ y_{\mathrm{i}}[k] &= \alpha\left(I_{\mathrm{i}}[k] + n_{\mathrm{i}}[k]\right) + \beta\left(I_{\mathrm{i}}[k] + n_{\mathrm{i}}[k]\right)^3 \\ &\quad + \beta\left(I_{\mathrm{i}}[k] + n_{\mathrm{i}}[k]\right)\left(I_{\mathrm{r}}[k] + n_{\mathrm{r}}[k]\right)^2. \qquad (99) \end{aligned}$$

Define $x_{\mathrm{r}}[k] \triangleq (I_{\mathrm{r}}[k] + n_{\mathrm{r}}[k])$ and $x_{\mathrm{i}}[k] \triangleq (I_{\mathrm{i}}[k] + n_{\mathrm{i}}[k])$. Then, (98) and (99) become

$$y_{\mathrm{r}}[k] = x_{\mathrm{r}}[k]\left(\alpha + \beta\left(x_{\mathrm{r}}^2[k] + x_{\mathrm{i}}^2[k]\right)\right) \qquad (100)$$

$$y_{\mathrm{i}}[k] = x_{\mathrm{i}}[k]\left(\alpha + \beta\left(x_{\mathrm{i}}^2[k] + x_{\mathrm{r}}^2[k]\right)\right). \qquad (101)$$

By dividing (101) by (100), we obtain

$$\frac{y_{\mathrm{i}}[k]}{y_{\mathrm{r}}[k]} = \frac{x_{\mathrm{i}}[k]}{x_{\mathrm{r}}[k]} = c[k] \qquad (102)$$

which yields

$$x_{\mathrm{i}}[k] = c[k]x_{\mathrm{r}}[k]. \qquad (103)$$

Substituting (103) in (100) gives

$$y_{\mathrm{r}}[k] = x_{\mathrm{r}}[k]\left(\alpha + \beta x_{\mathrm{r}}^2[k]\left(1 + c^2[k]\right)\right). \qquad (104)$$

Let

$$\beta_1[k] = \beta\left(1 + c^2[k]\right). \qquad (105)$$

Then

$$y_{\mathrm{r}}[k] = \alpha x_{\mathrm{r}}[k] + \beta_1[k]x_{\mathrm{r}}^3[k]. \qquad (106)$$

By rearranging (106), we get

$$x_{\mathrm{r}}^3[k] + \frac{\alpha}{\beta_1[k]}x_{\mathrm{r}}[k] - \frac{y_{\mathrm{r}}[k]}{\beta_1[k]} = 0. \qquad (107)$$

To solve the third order equation (107), we use the Cardano's method in [29] which gives the roots as

$$\begin{aligned} x_{\mathrm{r},l+1}[k] &= \kappa^l \sqrt[3]{-\frac{q[k]}{2} + \sqrt{\frac{q^2[k]}{4} + \frac{p^3[k]}{27}}} \\ &\quad + \kappa^{2l} \sqrt[3]{-\frac{q[k]}{2} - \sqrt{\frac{q^2[k]}{4} + \frac{p^3[k]}{27}}} \qquad (108) \end{aligned}$$

where $l = 0, 1, 2$, $p[k] = \frac{\alpha}{\beta_1[k]}$, $q = -\frac{y_{\mathrm{r}}[k]}{\beta_1[k]}$, $\kappa = -\frac{1}{2} + j\frac{\sqrt{3}}{2}$, $\kappa^2 = \overline{\kappa} = -\frac{1}{2} - j\frac{\sqrt{3}}{2}$ and $\kappa^4 = \kappa$.

Now, the second stage of the mapping has to decide which root is the best one. From (108), the three available roots could be all real or one real and two complex conjugate roots. Since $x_{\mathrm{r}}[k]$ is real, then in the latter case we pick the real root and discard the two complex ones. On the other hand, if the three roots are real, then we pick the root as follows:

1) Obtain an initial estimate for the channel taps $\hat{\mathbf{h}}_{\mathrm{int}}$ (will be discussed later in this section), with an average mean square error $\mathrm{MSE}_{\mathrm{int}} = \mathbb{E}\left\{\left\|\mathbf{h}_{\mathrm{int,err}}\right\|^2\right\}$.
2) Calculate

$$\hat{x}_{\mathrm{r,int}}[k] = \Re\left\{\hat{I}_{1,\mathrm{int}}\right\} = \Re\left\{\mathbf{u}^T[k]\hat{\mathbf{h}}_{\mathrm{int}}\right\} \qquad (109)$$

$$\hat{x}_{\mathrm{i,int}}[k] = \Im\left\{\hat{I}_{1,\mathrm{int}}\right\} = \Im\left\{\mathbf{u}^T[k]\hat{\mathbf{h}}_{\mathrm{int}}\right\}. \qquad (110)$$

3) Determine the distance between $\hat{x}_{\mathrm{int}} \triangleq \hat{x}_{\mathrm{r,int}} + j\hat{x}_{\mathrm{i,int}}$ and the three roots of (108) as

$$d_l[k] = \sqrt{(x_{\mathrm{r},l}[k] - \hat{x}_{\mathrm{r,int}}[k])^2 + (x_{\mathrm{i},l}[k] - \hat{x}_{\mathrm{i,int}}[k])^2} \qquad (111)$$

where $l = 1, 2, 3$.
4) Choose the root corresponding to the smallest distance as

$$x_{\mathrm{r}}^\dagger[k] = x_{\mathrm{r},l^\dagger}[k] \qquad (112)$$

where $l^\dagger = \arg_l \min(d_l)$. Then, from (103), we obtain $x_{\mathrm{i}}^\dagger[k] = c[k]\,x_{\mathrm{r}}^\dagger[k]$.

At a high input power, it is very probable that two roots become very close, and hence the wrong one could be picked. To cope with that problem, first we define the square of the distance between the nearest two roots to $\hat{x}_{\mathrm{int}}$ as

$$d_{\mathrm{near}}^2[k] = (x_{\mathrm{r},l_1}[k] - x_{\mathrm{r},l_2}[k])^2 + (x_{\mathrm{i},l_1}[k] - x_{\mathrm{i},l_2}[k])^2 \qquad (113)$$

where $x_{l_1}[k] \triangleq x_{\mathrm{r},l_1}[k] + jx_{\mathrm{i},l_1}[k]$ and $x_{l_2}[k] \triangleq x_{\mathrm{r},l_2}[k] + jx_{\mathrm{i},l_2}[k]$ are the nearest two roots to $\hat{x}_{\mathrm{int}}$. Then, we compare that squared distance with $P_{\mathrm{I}}\mathrm{MSE}_{\mathrm{int}}$, where P_{I} is the transmitted interference power, such that if $d_{\mathrm{near}}^2[k] < \rho P_{\mathrm{I}}\mathrm{MSE}_{\mathrm{int}}$,

the sample will be excised. ρ is a factor that we choose to excise the bad samples. To make the estimation more robust, we use $\rho = 5$. Additionally, if we find for a given frame of μ samples that more than 10% of the frame samples should be removed, we excise the whole frame.

Now, the equivalent linear system is given by

$$x^{\dagger}[k] = I[k] + n[k] \tag{114}$$

where

$$x^{\dagger}[k] \triangleq x_{\mathrm{r}}^{\dagger}[k] + j x_{\mathrm{i}}^{\dagger}[k] \tag{115}$$
$$I[k] \triangleq I_{\mathrm{r}}[k] + j I_{\mathrm{i}}[k] \tag{116}$$
$$n[k] \triangleq n_{\mathrm{r}}[k] + j n_{\mathrm{i}}[k]. \tag{117}$$

Suppose we use μ samples to estimate the channel. Then

$$\mathbf{x}^{\dagger} = \mathbf{I} + \mathbf{n} = \mathbf{U}\mathbf{h} + \mathbf{n} \tag{118}$$

where

$$\mathbf{x}^{\dagger} \triangleq \left[x^{\dagger}[k+\mu-1] \quad \cdots \quad x^{\dagger}[k+1] \quad x^{\dagger}[k] \right]^{T} \tag{119}$$
$$\mathbf{n} \triangleq \left[n[k+\mu-1] \quad \cdots \quad n[k+1] \quad n[k] \right]^{T} \tag{120}$$
$$\mathbf{I} \triangleq \left[I[k+\mu-1] \quad \cdots \quad I[k+1] \quad I[k] \right]^{T} \tag{121}$$
$$\mathbf{h} \triangleq \left[h_0 \quad \cdots \quad h_{L-2} \quad h_{L-1} \right]^{T} \tag{122}$$

and

$$\mathbf{U} \triangleq \begin{bmatrix} \mathbf{u}^{T}[k+\mu-1] \\ \vdots \\ \mathbf{u}^{T}[k] \end{bmatrix} \tag{123}$$
$$= \begin{bmatrix} u[k+\mu-1] & \cdots & u[k+\mu-L] \\ \vdots & \vdots & \vdots \\ u[k] & \cdots & u[k-L+1] \end{bmatrix}. \tag{124}$$

Finally, the least square estimation of $\mathbf{h}$ is given by

$$\hat{\mathbf{h}} = \left(\mathbf{U}^{H}\mathbf{U} \right)^{-1} \mathbf{U}^{H}\mathbf{x}^{\dagger}. \tag{125}$$

C. MECHANISM TO OBTAIN AN INITIAL ESTIMATE OF THE CHANNEL

Previously, we have mentioned that the UKF filter and the NL-L mapping algorithm need to have an initial estimate for the channel. Hence, we present two approaches to find an initial estimate of the channel.

In the first approach, we consider the proposed scenario in [13] which assumes a coordination between the RAS and the CWC system. Based on that coordination, we suggest that the CWC system can send a small packet of samples (say 1000 samples) at the beginning of each long transmission packet. This packet power is small, in order for the LNA to operate in its linear region. Thus, the RAS main receiver can simply obtain a good initial estimate of the channel.

In the second approach, we insert an auxiliary receiver chain and a switching mechanism to the main receiver such that the switch connects the main RAS antenna to either the auxiliary or the main receiver chain according to the switching control signal. The auxiliary receiver's LNA is designed to have a wider linear range so that during the phase of channel initial estimation, a reliable initial channel estimate is obtained from the auxiliary receiver chain. During normal RAS observation intervals, the switch connects the main RAS antenna to the main receiver.

IV. PERFORMANCE ANALYSIS FOR THE PROPOSED DETECTOR UNDER STRONG RFI AND CHANNEL ESTIMATION ERROR

In the last section, we have proposed a new detector to estimate the RAS signal power under the effect of the LNA nonlinearity. In this section, we provide a detailed performance analysis for the proposed detector. Throughout this section, we use the following assumptions/settings:

1) The time averaging is done over a very large number of samples. Thus, the averaging process approaches expectation.
2) The channel is a frequency-flat Rayleigh fading channel, i.e, $h = h_{\mathrm{r}} + jh_{\mathrm{i}} \sim CN(0,1)$. Then, the odd moments are zeros, $\mathbb{E}\{h_{\mathrm{r}}^2\} = \mathbb{E}\{h_{\mathrm{i}}^2\} = P_{\mathrm{h}}$, $\mathbb{E}\{h_{\mathrm{r}}^4\} = \mathbb{E}\{h_{\mathrm{i}}^4\} = 3P_{\mathrm{h}}^2$, $\mathbb{E}\{h_{\mathrm{r}}^6\} = \mathbb{E}\{h_{\mathrm{i}}^6\} = 15P_{\mathrm{h}}^3$ and $\mathbb{E}\{h_{\mathrm{r}}h_{\mathrm{i}}\} = 0$.
3) A least-square channel estimation based on μ samples is assumed where
$$\hat{h} = \hat{h}_{\mathrm{r}} + j\hat{h}_{\mathrm{i}} = \left(h_{\mathrm{r}} + h_{\mathrm{e,r}}\right) + j\left(h_{\mathrm{i}} + h_{\mathrm{e,i}}\right) \tag{126}$$
with $\mathbb{E}\{h_{\mathrm{e,r}}^2\} = \mathbb{E}\left\{h_{\mathrm{e,i}}^2\right\} = P_{\mathrm{e}} = \frac{1}{2\,\mu\,\mathrm{INR}}$, $\mathbb{E}\{h_{\mathrm{e,r}}^4\} = \mathbb{E}\left\{h_{\mathrm{e,i}}^4\right\} \approx 0$, $\mathbb{E}\{h_{\mathrm{e,r}}^6\} = \mathbb{E}\left\{h_{\mathrm{e,i}}^6\right\} \approx 0$ and $\mathbb{E}\{h_{\mathrm{r}}h_{\mathrm{e,r}}\} = \mathbb{E}\{h_{\mathrm{i}}h_{\mathrm{e,i}}\} = 0$.
4) The noise is a complex Gaussian noise with a constant power $2\sigma_{\mathrm{n}}^2 = -50$dBm. Thus, $\mathbb{E}\{n_{\mathrm{r}}^2\} = \mathbb{E}\{n_{\mathrm{i}}^2\} = \sigma_{\mathrm{n}}^2$, $\mathbb{E}\{n_{\mathrm{r}}^4\} = \mathbb{E}\{n_{\mathrm{i}}^4\} = 3\sigma_{\mathrm{n}}^4$ and $\mathbb{E}\{n_{\mathrm{r}}^6\} = \mathbb{E}\{n_{\mathrm{i}}^6\} = 15\sigma_{\mathrm{n}}^6$.
5) The interference has an average power P_{I}. Thus, from the previous assumption the interference to noise ratio (INR) is INR(dB) $= P_{\mathrm{I}}$(dBm) $- 50$. Any increase in the interference power makes the same increase in the INR.

Based on the above settings, we deduce that $\mathbb{E}\{C_1^2\} = \mathbb{E}\{D_1^2\}$, $\mathbb{E}\{C_2^2\} = \mathbb{E}\{D_2^2\}$, $\mathbb{E}\{C_3^2\} = \mathbb{E}\{D_3^2\}$, $\zeta_{\mathrm{r,res}} = \zeta_{\mathrm{i,res}} = 0$, $\mathbb{E}\{z_{\mathrm{r}}^2\} = \mathbb{E}\{z_{\mathrm{i}}^2\}$, $\mathbb{E}\{s_{\mathrm{r}}^2\} = \mathbb{E}\{s_{\mathrm{i}}^2\} = \frac{P_{\mathrm{s}}}{2}$ and $\mathbb{E}\{\xi_{\mathrm{r,res}}^2\} = \mathbb{E}\left\{\xi_{\mathrm{i,res}}^2\right\}$. Consequently, (57) becomes

$$\mathbb{E}\left\{z_{\mathrm{r}}^2\right\} = G_1\mathbb{E}\left\{s_{\mathrm{r}}^2\right\} + \mathbb{E}\left\{C_3^2\right\} + \mathbb{E}\left\{\xi_{\mathrm{r,res}}^2\right\} \tag{127}$$

where $G_1 = \left(\mathbb{E}\{C_1^2\} + \mathbb{E}\{C_2^2\}\right)$. Then, the estimated RAS signal power in (59) can be expressed as

$$\hat{P}_{\mathrm{s}} = \alpha_{\mathrm{nl}}P_{\mathrm{s}} + \alpha_{\mathrm{n}} + \alpha_{\mathrm{e}} \tag{128}$$

where $\alpha_{\mathrm{nl}} = \frac{G_1}{\hat{G}_1}$, $\alpha_{\mathrm{n}} = 2\frac{\mathbb{E}\{C_3^2\} - \mathbb{E}\left\{\hat{C}_3^2\right\}}{\hat{G}_1}$ and $\alpha_{\mathrm{e}} = \frac{2\mathbb{E}\{\xi_{\mathrm{r,res}}^2\}}{\hat{G}_1}$. So, $\hat{P}_{\mathrm{s}}$ is affected by the interference power level and the estimated channel since they affect α_{nl}, α_{n} and α_{e}.

Additionally, the interference at time instant k becomes

$$I[k] = \underbrace{(u_{\mathrm{r}}[k]h_{\mathrm{r}} - u_{\mathrm{i}}[k]h_{\mathrm{i}})}_{I_{\mathrm{r}}[k]} + j\underbrace{(u_{\mathrm{r}}[k]h_{\mathrm{i}} + u_{\mathrm{i}}[k]h_{\mathrm{r}})}_{I_{\mathrm{i}}[k]}. \quad (129)$$

Thus, the moments of the real and imaginary parts of the received interference are derived as

$$\mathbb{E}\left\{\hat{I}_{\mathrm{r}}^2[k]\right\} = \mathbb{E}\left\{\hat{I}_{\mathrm{i}}^2[k]\right\} = 2P_{\mathrm{u}}\left(P_{\mathrm{h}} + P_{\mathrm{e}}\right) \quad (130)$$

$$\mathbb{E}\left\{\hat{I}_{\mathrm{r}}^4[k]\right\} = \mathbb{E}\left\{\hat{I}_{\mathrm{i}}^4[k]\right\} = 2P_{\mathrm{u},4}\left(3P_{\mathrm{h}}^2 + 6P_{\mathrm{h}}P_{\mathrm{e}}\right) + 6P_{\mathrm{u}}^2\left(P_{\mathrm{h}}^2 + 2P_{\mathrm{h}}P_{\mathrm{e}}\right) \quad (131)$$

$$\mathbb{E}\left\{\hat{I}_{\mathrm{r}}^2[k]\hat{I}_{\mathrm{i}}^2[k]\right\} = 2P_{\mathrm{u},4}\left(P_{\mathrm{h}}^2 + 2P_{\mathrm{h}}P_{\mathrm{e}}\right) + 2P_{\mathrm{u}}^2P_{\mathrm{h}}^2 \quad (132)$$

$$\mathbb{E}\left\{\hat{I}_{\mathrm{r}}^6[k]\right\} = \mathbb{E}\left\{\hat{I}_{\mathrm{i}}^6[k]\right\} = 2P_{\mathrm{u},6}\left(15P_{\mathrm{h}}^3 + 45P_{\mathrm{h}}^2P_{\mathrm{e}}\right) + 30P_{\mathrm{u},4}P_{\mathrm{u}}\left(3P_{\mathrm{h}}^3 + 9P_{\mathrm{h}}^2P_{\mathrm{e}}\right) \quad (133)$$

where $P_{\mathrm{u}} = \mathbb{E}\left\{u_{\mathrm{r}}^2[k]\right\} = \mathbb{E}\left\{u_{\mathrm{i}}^2[k]\right\}$, $P_{\mathrm{u},4} = \mathbb{E}\left\{u_{\mathrm{r}}^4[k]\right\} = \mathbb{E}\left\{u_{\mathrm{i}}^4[k]\right\}$ and $P_{\mathrm{u},6} = \mathbb{E}\left\{u_{\mathrm{r}}^6[k]\right\} = \mathbb{E}\left\{u_{\mathrm{i}}^6[k]\right\}$. P_{u} is the same for QPSK and 16-QAM and equal to $\frac{P_{\mathrm{I}}}{2}$, but $P_{\mathrm{u},4}$ and $P_{\mathrm{u},6}$ are given by

$$P_{\mathrm{u},4} = \begin{cases} P_{\mathrm{u}}^2, & \mathrm{QPSK} \\ 1.64P_{\mathrm{u}}^2, & 16-\mathrm{QAM} \end{cases} \quad (134)$$

and

$$P_{\mathrm{u},6} = \begin{cases} P_{\mathrm{u}}^3, & \mathrm{QPSK} \\ 2.92P_{\mathrm{u}}^3, & 16-\mathrm{QAM} \end{cases} \quad (135)$$

To determine the effects of the interference power level (P_{u}) and the estimation block length (μ) on the RAS signal power estimation, we investigate how α_{nl}, α_{e} and α_{n} are affected by P_{u} and μ. First, we examine the effects of P_{u} and μ on $\hat{G}_1$, since it is a common term in all the terms we need to check. By applying the assumptions, and substituting (130), (131) and (132) into (47) and (49), we obtain

$$\hat{G}_1 = G_1 + \omega_{\mathrm{res}} \quad (136)$$

where

$$G_1 = \alpha^2 + 8\alpha\beta\left(2P_{\mathrm{u}}P_{\mathrm{h}} + \sigma_{\mathrm{n}}^2\right) + 10\beta^2\left(8P_{\mathrm{u},4}P_{\mathrm{h}}^2 + 8P_{\mathrm{u}}^2P_{\mathrm{h}}^2 + 16P_{\mathrm{u}}P_{\mathrm{h}}\sigma_{\mathrm{n}}^2\right) \quad (137)$$

$$\omega_{\mathrm{res}} = 8\alpha\beta\left(P_{\mathrm{u}}P_{\mathrm{e}}\right) + 10\beta^2\left(16P_{\mathrm{u},4}P_{\mathrm{h}}P_{\mathrm{e}} + 12P_{\mathrm{u}}^2P_{\mathrm{h}}P_{\mathrm{e}} + 16P_{\mathrm{u}}P_{\mathrm{e}}\sigma_{\mathrm{n}}^2\right). \quad (138)$$

Fig. 4 shows how $\hat{G}_1$ changes with the interference power under perfect channel estimation (i.e., $P_{\mathrm{e}} = 0$, hence $\omega_{\mathrm{res}} = 0$) and the RFI modulation of QPSK or 16-QAM. At low interference power, $\hat{G}_1$ is almost constant since the first term of G_1 namely α^2 dominates. With an increased interference power, the value of $\hat{G}_1$ begins to reduce due to the increasing magnitude of the second term beside $8\alpha\beta$, where β is negative, in G_1. As the interference power increases further, the third term of G_1, beside $10\beta^2$, begins to yield some effect. Since this term is positive, it reduces the effect of the second term. This effect can be easily noticed in the 16-QAM case since $P_{\mathrm{u},4}$ is higher in the 16-QAM than in the QPSK. As a result, the third term effect in the 16-QAM case appears earlier than in the QPSK case.

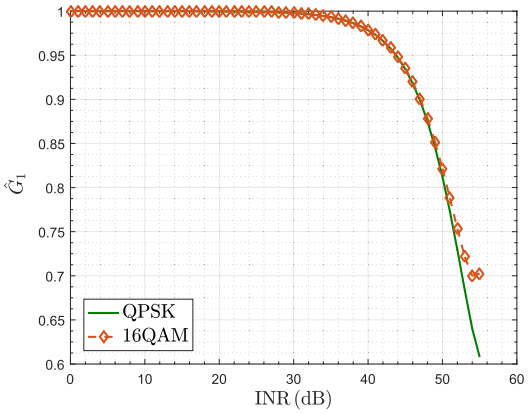

FIGURE 4. Effect of the interference power on $\hat{G}_1$ in a flat fading channel with a perfect channel estimation.

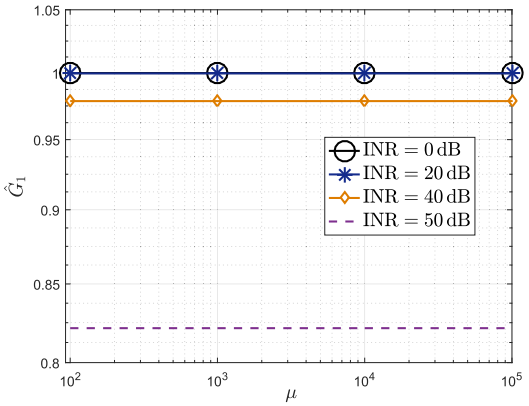

FIGURE 5. Effect of μ on $\hat{G}_1$ in a flat fading channel.

Fig. 5 reveals that μ has no effect on $\hat{G}_1$, even by changing the interference power. This can be easily explained since ω_{res} is dominated by $P_{\mathrm{u}}P_{\mathrm{e}} = \frac{\sigma_{\mathrm{n}}^2}{2\mu}$ which is negligible compared to G_1. Thus, $\hat{G}_1$ becomes constant with μ at the same interference level.

Fig. 6 demonstrates the effect of different values of μ on α_{nl} in (128) at different interference power values and the results are the same for QPSK and 16-QAM modulations. We observe that μ has almost no effect on α_{nl} which is constant at 1. This result was expected since we showed that μ has almost no effect on $\hat{G}_1$, hence $\hat{G}_1 \approx G_1$ and $\alpha_{\mathrm{nl}} \approx 1$. So, for the rest of this section we consider $\hat{G}_1 \approx G_1$.

Next, we discuss the effect of P_{u} and μ on α_{e} in (128). By squaring (41), taking the expectation, and then substituting (130), (131), (132) and (133), we obtain

$$\mathbb{E}\left\{\xi_{\mathrm{r,res}}^2\right\} = 2\alpha^2P_{\mathrm{u}}P_{\mathrm{e}} + 8\alpha\beta P_{\mathrm{u},4}P_{\mathrm{h}}P_{\mathrm{e}}\left(2P_{\mathrm{u},4} + 2P_{\mathrm{u}}^2\right) + 10\beta^2P_{\mathrm{h}}^2P_{\mathrm{e}}\left(8P_{\mathrm{u},6} + 24P_{\mathrm{u}}P_{\mathrm{u},4}\right). \quad (139)$$

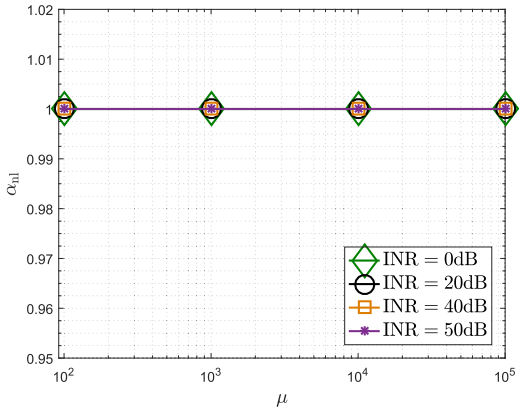

FIGURE 6. Effect of μ on α_{nl} with different INR values in a flat fading channel.

Then, α_e is given by (140) for QPSK and (141) for 16-QAM, both shown at the bottom of this page.

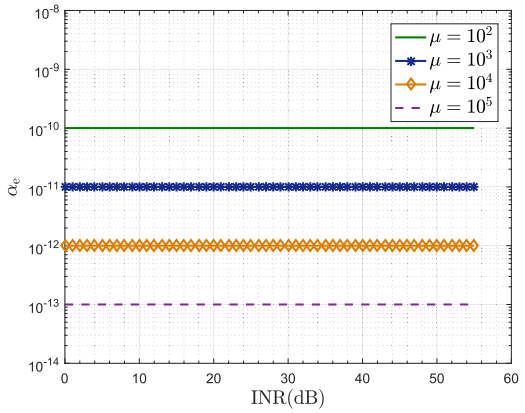

FIGURE 7. Effect of the interference power and μ on α_e in a flat fading channel using QPSK.

Fig. 7 shows the effect of μ and interference power on α_e for QPSK modulation. It is clear that the interference level has no effect on α_e but μ affects α_e. We can explain this from (140), where at low INR the terms with $\alpha\beta$ and β^2 are very small and can be neglected, thus $\alpha_e = 4P_uP_e$. At high INR, we can neglect the noise power σ_n^2, hence $\alpha_e = 4P_uP_e$ as in the low INR case. Since INR $= \frac{P_u}{\sigma_n^2}$, then $\alpha_e = \frac{2\sigma_n^2}{\mu}$, which is independent of the interference power and is inversely proportional to μ. The corresponding results for 16-QAM are similar to the QPSK case and the results are presented in a different setting in Fig. 8 which illustrates an inversely linear relationship of α_e on μ. A slight difference

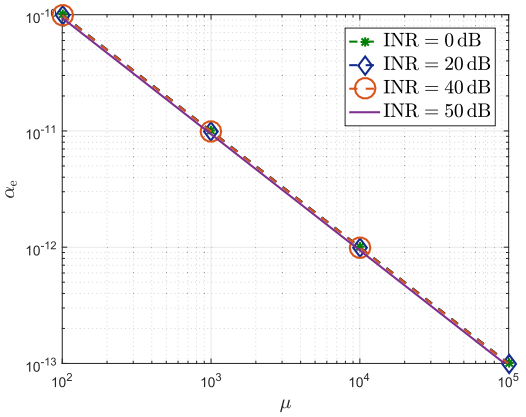

FIGURE 8. Effect of the interference power and μ on α_e in a flat fading channel using 16-QAM.

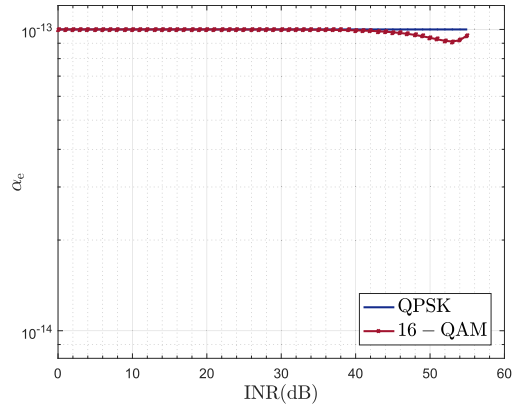

FIGURE 9. Effect of the interference power on α_e in a flat fading channel with $\mu = 10^5$.

between the QPSK and 16-QAM cases is shown in Fig. 9 where α_e for 16-QAM has a slight dip at very high INR which could be ascribed to different peak-to-average ratio characteristics of 16-QAM.

Finally, we show the effect of α_n on the detection process of the RAS signal power. Using (130), (131) and (132) in (47), we obtain

$$\mathbb{E}\left\{\hat{C}_3^2\right\} = \mathbb{E}\left\{C_3^2\right\} + \gamma_{res} \tag{142}$$

where

$$\begin{aligned}\mathbb{E}\left\{C_3^2\right\} &= \sigma_n^2\Big(\alpha^2 + 8\alpha\beta\left(2PP_h + \sigma_n^2\right) \\ &\quad + 10\beta^2\left(8P_4P_h^2 + 8P^2P_h^2 + 14.4PP_h\sigma_n^2\right)\Big)\end{aligned} \tag{143}$$

$$\alpha_e = 4P_uP_e\frac{\alpha^2 + 8\alpha\beta\left(2P_uP_h\right) + 10\beta^2\left(16P_u^2P_h^2\right)}{\alpha^2 + 8\alpha\beta\left(2P_uP_h + \sigma_n^2\right) + 10\beta^2\left(16P_u^2P_h^2 + 16PP_h\sigma_n^2\right)}, \quad \text{QPSK.} \tag{140}$$

$$\alpha_e = 4P_uP_e\frac{\alpha^2 + 8\alpha\beta\left(2.64P_uP_h\right) + 10\beta^2\left(31.36P_u^2P_h^2\right)}{\alpha^2 + 8\alpha\beta\left(2P_uP_h + \sigma_n^2\right) + 10\beta^2\left(21.12P_u^2P_h^2 + 16PP_h\sigma_n^2\right)}, \quad 16-\text{QAM.} \tag{141}$$

$$\gamma_{\text{res}} = \sigma_{\text{n}}^2\Big(8\alpha\beta\,(PP_{\text{e}}) + 10\beta^2\left(16P_4P_{\text{h}}P_{\text{e}} + 12P^2P_{\text{h}}P_{\text{e}} + 14.4PP_{\text{e}}\sigma_{\text{n}}^2\right)\Big). \tag{144}$$

Then, $\alpha_{\text{n}} = \frac{2\gamma_{\text{res}}}{G_{\text{l}}}$. In case of QPSK, γ_{res} becomes

$$\gamma_{\text{res}} = 2P_{\text{u}}P_{\text{e}}\sigma_{\text{n}}^2\left(8\alpha\beta + 28P_{\text{u}}P_{\text{h}} + 14.4P_{\text{u}}\sigma_{\text{n}}^2\right) = \frac{2\left(\sigma_{\text{n}}^2\right)^2}{\mu}\left(8\alpha\beta + 28P_{\text{u}}P_{\text{h}} + 14.4P_{\text{u}}\sigma_{\text{n}}^2\right). \tag{145}$$

From (145), we observe that α_{n} is inversely proportional to μ like α_{e} is. In addition, we notice that α_{n} is proportional to $\left(\sigma_{\text{n}}^2\right)^2$ while α_{e} is proportional to σ_{n}^2. Hence, α_{n} can be neglected. The same conclusion is valid for the 16-QAM case.

Based on this analytical evaluation, we conclude that α_{e} is the main effective parameter in the detection process, and we will show that by numerical results in the next section.

V. NUMERICAL RESULTS

In this section, we present some numerical results to illustrate the effectiveness of our proposed methods for channel estimation and RAS signal power detection. Throughout this section, we use the same LNA parameters that was mentioned in section II-B, where $a_1 = 1$ and $a_3 = -72.5$. The noise power is $P_{\text{n}} = |n_{\text{bb}}[k]|^2 = -50$ dBm and interference power is $P_{\text{I}} = |I_{1,\text{bb}}[k]|^2$. Hence, $P_{\text{I}}(\text{dBm}) = \text{INR}(\text{dB}) - 50$ where INR is the interference to noise ratio. In our simulations, we consider a quasi-static Rayleigh fading environment, where the channel is considered constant over a frame of μ samples. In the simulations, we use two different channel models. The first is a flat fading channel (one tap) that we call ''channel (a)'', while the other is a six-tap channel with a 3-dB per tap decaying exponential power delay profile, which we call ''channel (b)''. For the detection of the RAS signal power, we perform our simulations by considering a signal power at 10 dB below the noise power and an averaging window of 10^7 samples.

A. CHANNEL ESTIMATION PERFORMANCE IN A NONLINEAR SYSTEM

In this subsection, we compute the average mean square error for the estimate of the interferene channel at the main receiver $\text{MSE}_{\text{h}} = \overline{\left\|\mathbf{h} - \hat{\mathbf{h}}\right\|^2}$, when the received signal suffers from the LNA nonlinearity. We evaluate three methods: UKF, NL-L mapping and a least square method (LS) [27]. The results of these techniques are compared with the ideal case, where the LNA is linear (i.e, $a_3 = 0$) and we use an LS to estimate the channel. For both UKF and NL-L mapping methods, we deduce an initial channel estimation with 1000 samples at INR = 30 dB. Additionally, we neglect the RAS signal since it is much below the noise level.

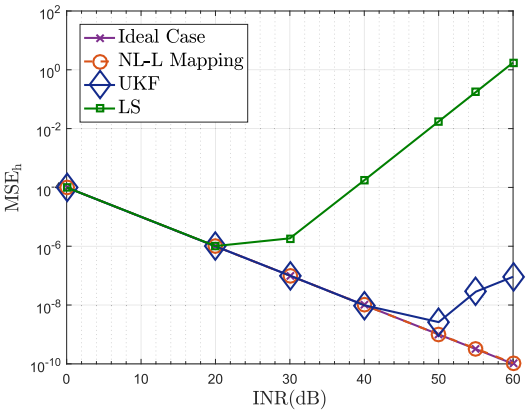

FIGURE 10. Comparison between channel estimation techniques in channel (a) with QPSK interference modulation.

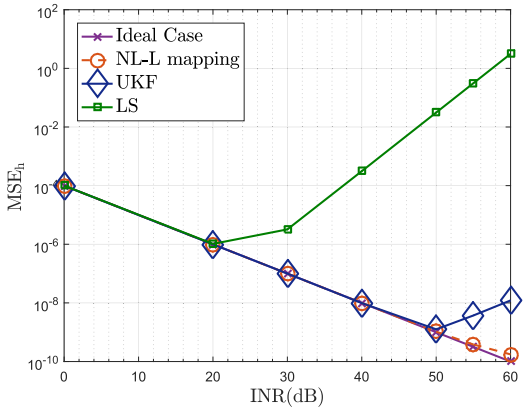

FIGURE 11. Comparison between channel estimation techniques in channel (a) with 16-QAM interference modulation.

Fig. 10, Fig. 11, Fig. 12 and Fig. 13 exhibit the MSE_{h} of the channel estimates for the two channels and two modulations. We observe that at low transmitted power, the MSE_{h} of the channel estimates using UKF, NL-L mapping and LS are the same as the MSE_{h} of the ideal case. When the INR increases, the MSE_{h} of the LS channel estimate begins to diverge and increases dramatically. On the other hand, the MSE_{h} of the two proposed estimators coincide with the MSE_{h} of the ideal case. When the interference power reaches near the 1-dB compression point, the MSE_{h} of the UKF method begins to deviate from the ideal MSE_{h}. On contrary, we notice that the MSE_{h} of the NL-L mapping approach is almost the same as the MSE_{h} of the ideal case. From these results, we can conclude that our proposed NL-L mapping outperforms the least square and the UKF and it is robust at high interference power.

B. RAS SIGNAL DETECTION PERFORMANCE IN A NONLINEAR SYSTEM

In this subsection, we present the robustness of our RAS signal power detection in the presence of a high-level interference, which shifts the LNA to its non-linear region. In order to focus on the effect of the RAS signal power detection method, we assume that we have perfectly estimated the channel

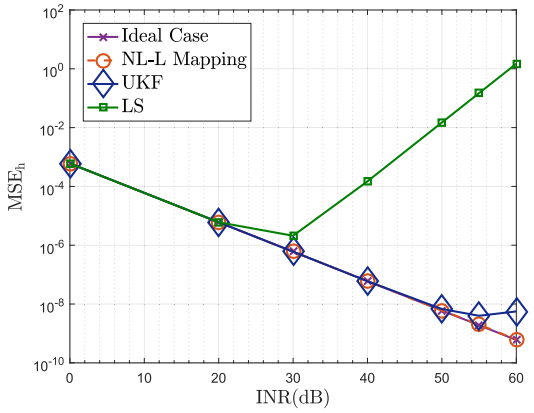

FIGURE 12. Comparison between channel estimation techniques in channel (b) with QPSK interference modulation.

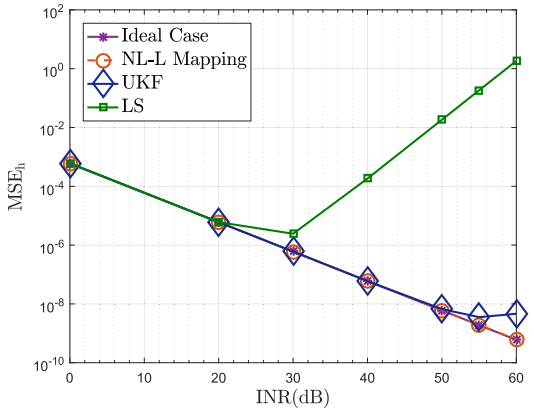

FIGURE 13. Comparison between channel estimation techniques in channel (b) with 16-QAM interference modulation.

at the receiver. Barnbaum and Bradley [18] used the LMS filter to estimate and remove the interference, followed by a conventional detector as in (6). Since the channel is known, the Weiner filter can be used instead of the LMS. Since the system is nonlinear, we have developed a formula for the Weiner filter coefficients which is shown in (150). By using these coefficients, (34) and (36) become

$$z_{\mathrm{r}}[k] = y_{\mathrm{r}}[k] - \Re\{\mathbf{W}_{\mathrm{opt}}^{T}[k]\mathbf{I}_{\mathrm{w}}[k]\} \tag{146}$$

and

$$z_{\mathrm{i}}[k] = y_{\mathrm{i}}[k] - \Im\{\mathbf{W}_{\mathrm{opt}}^{T}[k]\mathbf{I}_{\mathrm{w}}[k]\} \tag{147}$$

where

$$\mathbf{W}_{\mathrm{opt}}[k] = [w_{\mathrm{opt}}[k], \cdots, w_{\mathrm{opt}}[k-L+1]]^{T} \tag{148}$$

and

$$\mathbf{I}_{\mathrm{w}}[k] = [I[k], \cdots, I[k-L+1]]^{T}. \tag{149}$$

In this subsection, we investigate the behavior of the absolute mean normalized error ($\overline{e_{\mathrm{norm}}}$) with respect to the RFI power in four cases. These cases vary in the type of the LNA used (Linear or Nonlinear), the interference cancellation scheme used and the RAS signal power detector. In case 1 (ideal case), we use a linear LNA, while in the other cases we use a nonlinear LNA. In case 2 and 3, we excise the higher order interference terms as in (34) and (36). In case 1, we remove the first order interference term since the system is linear, while in case 4 we remove the interference using the derived Weiner filter as in (146) and (147). Finally for the RAS signal power detector, we use the conventional detector (6) in cases 1, 3 and 4, while we use our proposed one (58) in case 2. The four cases are summarized in Table 2.

TABLE 2. Cases used in simulation.

Case	LNA	Interference Cancellation	RAS Detector
1 (ideal)	Linear (2)	First order interference removal (4)	Conventional (6)
2	NL (11)	Higher order interference removal (34) & (36)	Proposed (59)
3	NL (11)	Higher order interference removal (34) & (36)	Conventional (6)
4	NL (11)	Wiener	Conventional (6)

The results for $\overline{e_{\mathrm{norm}}}$ are presented in Fig. 14, Fig. 15, Fig. 16, and Fig. 17 for the two channel models and two modulation schemes.

We observe that at low INR, $\overline{e_{\mathrm{norm}}}$ of the four cases are almost the same. As INR increases, $\overline{e_{\mathrm{norm}}}$ of cases 3 and 4 begin to diverge from the ideal case and increase drastically. On the other hand, $\overline{e_{\mathrm{norm}}}$ of case 2 coincides with the result of the ideal case as INR increases. When INR reaches a very high region, the $\overline{e_{\mathrm{norm}}}$ of case 2 slightly diverges from the ideal case. The reason for that slight divergence is that in the ideal case the averaging error (ζ_{res}) is divided by α^2 which is always constant, while in case 2 it is divided by G_1 which is slightly decreased by inducing more interference

$$\begin{aligned} w_{\mathrm{opt}}[k] = {} & \alpha h_{r,k} + \beta\frac{P_{\mathrm{I}}}{2}\left(h_{r,k}^3 + h_{r,k}h_{i,k}^2 + 3h_{r,k}\sum_{\substack{n=0\\n\neq k}}^{L-1} h_{r,n}^2 + 3h_{r,k}\sum_{l=0}^{L-1} h_{i,l}^2 + 2h_{i,k}\sum_{n=0,n\neq k}^{L-1} h_{r,n}h_{i,n} + h_{r,k}\sum_{\substack{n=0\\n\neq k}}^{L-1} h_{i,n}^2\right) \\ & + \beta\frac{P_{\mathrm{I}}}{2}\left(h_{r,k}\sum_{l=0}^{L-1} h_{r,l}^2 - 2h_{i,k}\sum_{l=0}^{L-1} h_{r,l}h_{i,l}\right) + j\left(\alpha h_{i,k} + \beta\frac{P_{\mathrm{I}}}{2}\left(h_{i,k}^3 + h_{i,k}h_{r,k}^2 + 3h_{i,k}\sum_{\substack{n=0\\n\neq k}}^{L-1} h_{i,n}^2\right)\right) \\ & + j\beta\frac{P_{\mathrm{I}}}{2}\left(3h_{i,k}\sum_{l=0}^{L-1} h_{r,l}^2 + 2h_{r,k}\sum_{\substack{n=0\\n\neq k}}^{L-1} h_{i,n}h_{r,n} + h_{i,k}\sum_{\substack{n=0\\n\neq k}}^{L-1} h_{r,n}^2 + h_{i,k}\sum_{l=0}^{L-1} h_{i,l}^2 - 2h_{r,k}\sum_{l=0}^{L-1} h_{i,l}h_{r,l}\right) \end{aligned} \tag{150}$$

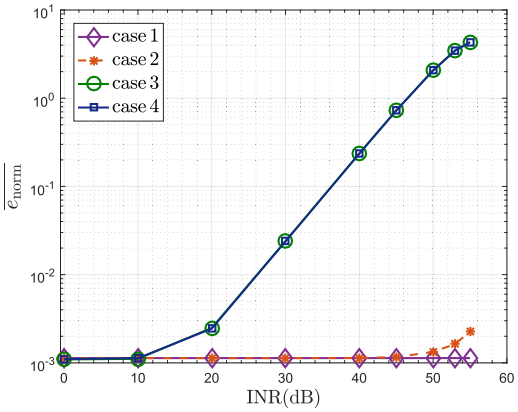

FIGURE 14. RAS signal detection performance in channel (a) (perfectly known) with a QPSK interference.

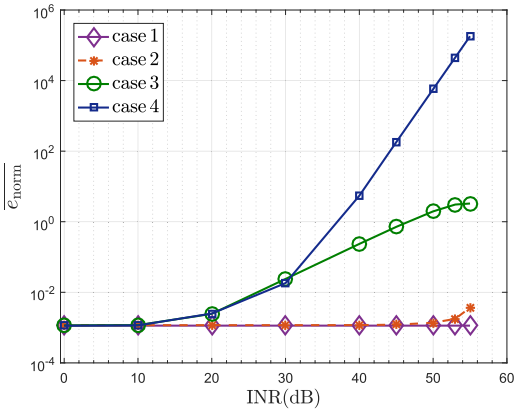

FIGURE 15. RAS signal detection performance in channel (a) (perfectly known) with a 16-QAM interference.

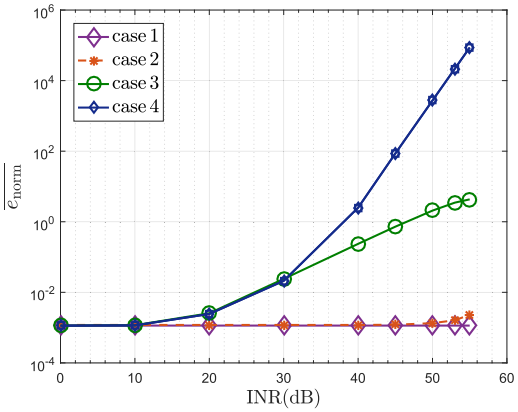

FIGURE 16. RAS signal detection performance in channel (b) (perfectly known) with a QPSK interference.

power. From these results we can conclude that our proposed RAS signal power detection scheme almost reaches the ideal detector performance.

C. COMBINED CHANNEL ESTIMATION AND RAS SIGNAL DETECTION PERFORMANCE

In the previous subsections, we have concluded that the NL-L mapping based channel estimator yields the best practical performance and the proposed RAS signal power detector

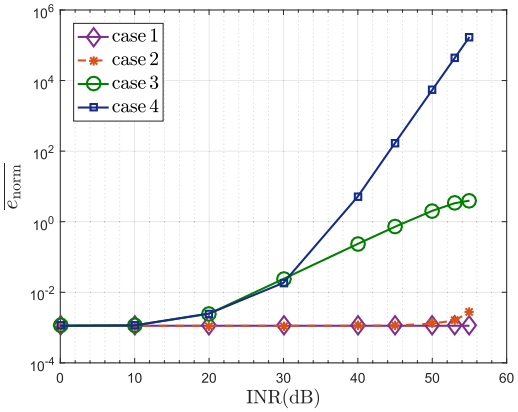

FIGURE 17. RAS signal detection performance in channel (b) (perfectly known) with a 16-QAM interference.

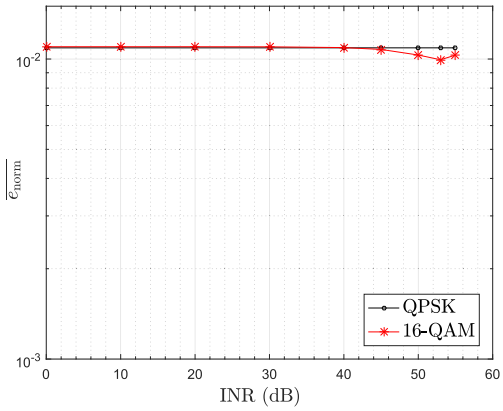

FIGURE 18. RAS signal detection in a flat fading channel using our proposed detection method with the NL-L mapping for both QPSK and 16-QAM.

outperforms the conventional one. In this subsection, we evaluate the performance of our proposed RAS signal power detector using our NL-L mapping channel estimation technique. Fig. 18 shows the average normalized error for the estimated RAS signal power ($\overline{e_{\text{norm}}}$) with channel (a) and by using QPSK and 16-QAM as RFI modulations, where the channel is constant over $\mu = 1000$ samples only. We can observe that α_{e} is the dominant error, where $\overline{e_{\text{norm}}}$ behavior with respect to the interference level is almost the same as α_{e}'s behavior in Fig. 9. Although the effect of that error can be decreased by increasing μ, the integration window in real RAS receivers is larger than what we used in our simulations. Thus, we can conclude that the residual interference is the dominant one in the RAS signal power detection.

VI. CONCLUSIONS

To mitigate an increasing conflict of spectrum access between RAS and CWC, we have explored a more aggressive spectrum access scenario where both CWC and RAS systems coordinate and simultaneously access the spectrum for some duration of time, and RAS is equipped with RFI cancellation. We have developed a new signal model under strong RFI and analyzed corresponding RAS signal detection performance.

Our study shows that strong RFI causes nonlinear distortions and severely degrades the performance of the conventional RAS signal power estimator. We also proposed an auxiliary receiver assisted nonlinear-RFI cancellation scheme, two channel estimators, and a modified RAS signal power estimator for the scenario with strong RFI. Our performance evaluation results clearly demonstrate substantial performance advantage of the proposed approaches over the existing approaches, and the need for incorporating nonlinear system model into the channel estimation, interference cancellation, and the RAS signal power estimation.

REFERENCES

[1] *Protection Creteria Used for Radio Astronomical Measurements*, document Rec. RA.769-2, ITU, Mar. 2003.
[2] L. Belostotski, J. W. Haslett, and B. Veidt, "Wide-band CMOS low noise amplifier for applications in radio astronomy," in *Proc. IEEE Int. Symp. Circuits Syst.*, May 2006, p. 4.
[3] S.-H. Weng, C.-H. Lin, H.-Y. Chang, and C.-C. Chiong, "Q-band low noise amplifiers using a 0.15μm MHEMT process for broadband communication and radio astronomy applications," in *IEEE MTT-S Int. Microw. Symp. Dig.*, Jun. 2008, pp. 455–458.
[4] Ó. Garcia-Perez, D. Segovia-Vargas, L. E. Garcia-Munoz, J. L. Jimenez-Martin, and V. Gonzalez-Posadas, "Broadband differential low-noise amplifier for active differential arrays," *IEEE Trans. Microw. Theory Techn.*, vol. 59, no. 1, pp. 108–115, Jan. 2011.
[5] B. A. Abelan *et al.*, "412- and 2534-GHz cryogenic mHEMT MMIC low-noise amplifiers," *IEEE Trans. Microw. Theory Techn.*, vol. 60, no. 12, pp. 4080–4088, Dec. 2012.
[6] W. Ciccognani, S. Colangeli, E. Limiti, and L. Scucchia, "Millimeter wave low noise amplifier for satellite and radio-astronomy applications," in *Proc. IEEE 1st AESS Eur. Conf. Satellite Telecommun. (ESTEL)*, Oct. 2012, pp. 1–4.
[7] J. Schleeh, N. Wadefalk, P. Nilsson, J. P. Starski, and J. Grahn, "Cryogenic broadband ultra-low-noise MMIC LNAs for radio astronomy applications," *IEEE Trans. Microw. Theory Techn.*, vol. 61, no. 2, pp. 871–877, Feb. 2013.
[8] Y. C. Chen, Y. Wang, C. C. Chiong, and H. Wang, "An ultra-broadband low noise amplifier in GaAs 0.1-μm pHEMT process for radio astronomy application," in *Proc. IEEE Int. Symp. Radio-Freq. Integr. Technol. (RFIT)*, Aug. 2017, pp. 80–82.
[9] *Preferred Frequency Bands for Radio Astronomical Measurements*, document Rec. RA.314-10, ITU, Jun. 2003.
[10] *Space Research Earth Station and Radio Astronomy Reference Antenna Radiation Pattern for Use in Interference Calculations, Including Coordination Procedures, for Frequencies Less Than 30 GHz*, document SA.509-3, ITU, Dec. 2013.
[11] *Levels of Data Loss to Radio Astronomy Observations and Percentage-of-Time Criteria Resulting From Degradation by Interference for Frequency Bands Allocated to the Radio Astronomy Service on a Primary Basis*, document Rec. RA.1513-2, ITU, Mar. 2015.
[12] *Protection of the Radio Astronomy Service in Frequency Bands Shared With Other Services*, document Rec. RA.1031-2, ITU, Jun. 2007.
[13] H. Minn, Y. R. Ramadan, and Y. Dai, "A new shared spectrum access paradigm between cellular wireless communications and radio astronomy," in *Proc. Global Commun. Conf. (GLOBECOM)*, Dec. 2016, pp. 1–6.
[14] Y. R. Ramadan, H. Minn, and Y. Dai, "A new paradigm for spectrum sharing between cellular wireless communications and radio astronomy systems," *IEEE Trans. Commun.*, vol. 65, no. 9, pp. 3985–3999, Sep. 2017.
[15] W. A. Baan, "RFI mitigation in radio astronomy," in *Proc. 30th Gen. Assembly Sci. Symp. URSI*, Oct. 2011, pp. 1–2.
[16] J. M. Ford and K. D. Buch, "RFI mitigation techniques in radio astronomy," in *Proc. IEEE Int. Geosci. Remote Sens. Symp. (IGARSS)*, Jul. 2014, pp. 231–234.
[17] *Techniques for Mitigation of Radio Frequency Interference in Radio Astronomy*, document RA.2126-1, ITU, Nov. 2013.
[18] C. Barnbaum and R. Bradley, "A new approach to interference excision in radio astronomy: Real-time adaptive cancellation," *Astron. J.*, vol. 115, pp. 2598–2614, Nov. 1998.
[19] A. J. Poulsen, B. D. Jeffs, K. F. Warnick, and J. R. Fisher, "Programmable real-time cancellation of GLONASS interference with the green bank telescope," *Astron. J.*, vol. 130, pp. 2916–2927, Dec. 2005.
[20] F. H. Briggs, J. F. Bell, and M. J. Kesteven, "Removing radio interference from contaminated astronomical spectra using an independent reference signal and closure relations," *Astron. J.*, vol. 120, no. 6, pp. 3351–3361, Dec. 2000.
[21] S. J. Julier, J. K. Uhlmann, and H. F. Durrant-Whyte, "A new approach for filtering nonlinear systems," in *Proc. Amer. Control Conf.*, Jun. 1995, pp. 1628–1632.
[22] S. J. Julier and J. K. Uhlmann, "New extension of the Kalman filter to nonlinear systems," *Proc. SPIE*, vol. 3068, pp. 182–194, Jul. 1997.
[23] S. J. Julier and J. K. Uhlmann, "Unscented filtering and nonlinear estimation," *Proc. IEEE*, vol. 92, no. 3, pp. 401–422, Mar. 2004.
[24] M. E. Abdelgelil and H. Minn, "Non-linear interference cancellation for radio astronomy receivers with strong RFI," in *Proc. IEEE Global Commun. Conf. (GLOBECOM)*, Dec. 2017, pp. 1–6.
[25] M. E. Tiuri, "Radio astronomy receivers," *IEEE Trans. Military Electron.*, vol. 8, no. 3, pp. 264–272, Jul. 1964.
[26] B. Razavi, "RF microelectronics," in *Basic Concepts in RF Design* (Communications Engineering and Emerging Technologies Series), 2nd ed. Upper Saddle River, NJ, USA: Prentice-Hall, 2011.
[27] S. M. Kay, *Fundamentals of Statistical Signal Processing, Estimation Theory (V. 1)*, vol. 1. Englewood Cliffs, NJ, USA: Prentice-Hall, 1993.
[28] S. S. Haykin, *Neural Networks and Learning Machines*, vol. 3. Upper Saddle River, NJ, USA: Pearson, 2009.
[29] B. P. Lathi, *Signal Processing and Linear Systems*. New York, NY, USA: Oxford Univ. Press, 1998.

MAHMOUD E. ABDELGELIL (S'17) received the B.S. (Hons.) and M.S. degrees in electronics and communications engineering from Cairo University, Giza, Egypt, in 2011 and 2014, respectively. He is currently pursuing the Ph.D. degree in electrical engineering with The University of Texas at Dallas, Richardson, TX, USA. His research interests include RFI cancellation for radio astronomy, wireless communications, signal processing, channel estimation, and control.

HLAING MINN (S'99–M'01–SM'07–F'16) received the B.E. degree in electrical electronic engineering from the Yangon Institute of Technology, Yangon, Myanmar, in 1995, the M.E. degree in telecommunications from the Asian Institute of Technology, Thailand, in 1997, and the Ph.D. degree in electrical engineering from the University of Victoria, Victoria, BC, Canada, in 2001. He was a Post-Doctoral Fellow with the University of Victoria in 2002. He has been with The University of Texas at Dallas, USA since 2002, where he is currently a Full Professor. His research interests include wireless communications, signal processing, signal design, dynamic spectrum access and sharing, next-generation wireless technologies, and bio-medical signal processing.

Dr. Minn served as a technical program committee member for over 30 IEEE conferences. He served as the Technical Program Co-Chair for the Wireless Communications Symposium of the IEEE GLOBECOM 2014 and the Wireless Access Track of the IEEE VTC, Fall 2009. He served as an Editor for the IEEE TRANSACTIONS ON COMMUNICATIONS from 2005 to 2016. He was also an Editor for the *International Journal of Communications and Networks* from 2008 to 2015. He has been serving as an Editor-at-Large for the IEEE TRANSACTIONS ON COMMUNICATIONS since 2016.